HHS Public Access

Author manuscript

Nat Immunol. Author manuscript; available in PMC 2020 September 04.

Published in final edited form as:

Nat Immunol. 2019 September ; 20(9): 1231–1243. doi:10.1038/s41590-019-0441-y.

PD-1 blockade in subprimed CD8 cells induces dysfunctional PD-1^{+}CD38^{hi} cells and anti-PD-1 resistance

Vivek Verma[1,11], **Rajeev K Shrimali**[1,12], **Shamim Ahmad**[1,13], **Winjie Dai**[1], **Hua Wang**[1], **Sumin Lu**[1], **Rahul Nandre**[1,11], **Pankaj Gaur**[1,11], **Jose Lopez**[11], **Moshe Sade-Feldman**[2,3], **Keren Yizhak**[3], **Stacey L. Bjorgaard**[2,3], **Keith T. Flaherty**[2], **Jennifer A. Wargo**[4], **Genevieve M. Boland**[5], **Ryan J. Sullivan**[2], **Gad Getz**[2,3,6], **Scott A. Hammond**[7], **Ming Tan**[8], **Jingjing Qi**[9], **Phillip Wong**[9], **Taha Merghoub**[9,10], **Jedd Wolchok**[9,10], **Nir Hacohen**[2,3], **John E. Janik**[1,14], **Mikayel Mkrtichyan**[1,11,15], **Seema Gupta**[1,11], **Samir N. Khleif**[1,11,*]

[1]Georgia Cancer Center, Augusta University, Augusta, GA, USA.

[2]Department of Medicine, Massachusetts General Hospital Cancer Center, Boston, MA, USA.

[3]Broad Institute of Massachusetts Institute of Technology and Harvard, Cambridge, MA, USA.

[4]Department of Surgical Oncology, University of Texas MD Anderson Cancer Center, Houston, TX, USA.

[5]Department of Surgery, Massachusetts General Hospital, Boston, MA, USA.

[6]Department of Pathology, Massachusetts General Hospital, Boston, MA, USA.

[7]MedImmune LLC, Gaithersburg, MD, USA.

[8]Department of Biostatistics, Bioinformatics & Biomathematics, Georgetown University, Washington, DC, USA.

[9]Memorial Sloan Kettering Cancer Center, New York, NY, USA.

[10]Weill Cornell Medical and Graduate Schools, New York, NY, USA.

[11]Present address: Lombardi Comprehensive Cancer Center, Georgetown University Medical Center, Washington, DC, USA.

---

[*]**Correspondence and requests for materials** should be addressed to S.N.K. snk48@georgetown.edu.

Author contributions

V.V., S.G. and S.N.K. were the main investigators and take primary responsibility for the paper. V.V., S.G. and S.N.K. were involved in the conception and design of the study, development of the methodology, analysis and interpretation of the data, administrative, technical or material support and writing and reviewing the manuscript. V.V. performed the experiments with assistance from R.K.S., S.A., W.D., H.W., S.L., R.N., P.G. and J.L. J.E.J. and M.M. helped review the manuscript. The acquisition of human tumor samples and their analysis were performed by M.S.-F., K.Y., S.L.B., K.T.F., J.A.W., G.M.B., R.J.S., G.G. and N.H. The acquisition of human PBMC samples and their analysis were performed by J.Q., P.W., T.M. and J.W. M.T. performed the statistical analysis of the human data. S.A.H. provided the anti-PD-1 antibody.

Online content

Any methods, additional references, Nature Research reporting summaries, source data, statements of code and data availability and associated accession codes are available at https://doi.org/10.1038/s41590–019-0441-y.

Supplementary information is available for this paper at https://doi.org/10.1038/s41590–019-0441-y.

Peer review information: Zoltan Fehervari was the primary editor on this article and managed its editorial process and peer review in collaboration with the rest of the editorial team.

[12]Present address: Therapeutic Discovery, MD Anderson Cancer Center, Houston, TX, USA.

[13]Present address: Five Prime Therapeutics Inc., South San Francisco, CA, USA.

[14]Present address: Incyte Inc., Wilmington, DE, USA.

[15]Present address: A2 Biotherapeutics, Agoura Hills, CA, USA.

Abstract

Understanding resistance to antibody to programmed cell death protein 1 (PD-1; anti-PD-1) is crucial for the development of reversal strategies. In anti-PD-1-resistant models, simultaneous anti-PD-1 and vaccine therapy reversed resistance, while PD-1 blockade before antigen priming abolished therapeutic outcomes. This was due to induction of dysfunctional PD-1^{+}CD38^{hi} CD8^{+} cells by PD-1 blockade in suboptimally primed CD8 cell conditions induced by tumors. This results in erroneous T cell receptor signaling and unresponsiveness to antigenic restimulation. On the other hand, PD-1 blockade of optimally primed CD8 cells prevented the induction of dysfunctional CD8 cells, reversing resistance. Depleting PD-1^{+}CD38^{hi} CD8^{+} cells enhanced therapeutic outcomes. Furthermore, non-responding patients showed more PD-1^{+}CD38^{+}CD8^{+} cells in tumor and blood than responders. In conclusion, the status of CD8^{+} T cell priming is a major contributor to anti-PD-1 therapeutic resistance. PD-1 blockade in unprimed or suboptimally primed CD8 cells induces resistance through the induction of PD-1^{+}CD38^{hi} CD8^{+} cells that is reversed by optimal priming. PD-1^{+}CD38^{hi} CD8^{+} cells serve as a predictive and therapeutic biomarker for anti-PD-1 treatment. Sequencing of anti-PD-1 and vaccine is crucial for successful therapy.

Signaling through programmed cell death protein 1 (PD-1) and its ligand, programmed cell death 1 ligand 1 (PD-L1), is an important immune checkpoint mechanism to maintain tolerance to self-antigens and prevent autoimmune diseases[1,2]. However, cancers use this mechanism to promote immune escape[3,4]. Accordingly, the immunotherapy of cancer patients using anti-PD-1 and PD-L1 antibodies has shown substantial clinical response[5,6], albeit only in a subset of cancer patients[7], necessitating the understanding of mechanisms of resistance. Resistance could be due to gene mutations, PD-L1 expression or other mechanisms that do not allow T cell activation in the tumor microenvironment (TME)[8]. Therefore, to overcome resistance, strategies using anti-PD-1 or anti-PD-L1 antibodies in combination with immune-activating agents, such as vaccines, are being developed[7,9–13].

Cancer vaccines, including neoantigens, are currently being explored in combination with anti-PD-1 and anti-PD-L1 antibodies in several clinical trials with the intent to reinvigorate T cell-mediated tumor killing and enhance the anti-PD-1 effect[14]. However, since the PD-1 pathway plays an important role in the balance of T cell activation and tolerance[15,16], identifying the optimal timing or sequencing of PD-1 blockade with respect to T cell receptor (TCR) engagement and the status of T cell priming is essential to achieve maximum therapeutic benefits. Moreover, anti-PD-1 is frequently administered before vaccine therapy in cancer patients for logistical reasons, such as the time required to develop tumor-specific vaccines. Therefore, we tested the ability of vaccination to reverse anti-PD-1 resistance and

different sequencing of the PD-1 blockade and antigen-specific vaccination in mouse tumor models that are known to be resistant to anti-PD-1 therapy[10,17].

Here we report a new mechanism of resistance to anti-PD-1 therapy. We show that PD-1 blockade in suboptimally primed $CD8^+$ T cell conditions results in the generation of dysfunctional $PD\text{-}1^+CD38^{hi}$ $CD8^+$ cells[18], leading to resistance to anti-PD-1 antibody and therapeutic failure. On the other hand, optimal antigenic stimulation reverses anti-PD-1 resistance. These results suggest that (1) treatment with anti-PD-1 in suboptimal priming conditions confers resistance to immunotherapy that can be reversed by proper antigen stimulation and (2) appropriate sequencing of immunomodulatory agents is crucial for therapeutic outcomes. We also show that a high frequency of $PD\text{-}1^+CD38^{hi}$ $CD8^+$ in both tumor and blood can serve as a biomarker of anti-PD-1 resistance as well as being used to select patients for anti-PD-1 therapy.

Results

PD-1 blockade before antigen priming with cancer vaccine abrogates antitumor immune effects

We first tested the effect of sequencing a tumor vaccine and PD-1 blockade on therapeutic outcome using two syngeneic mouse tumor models, TC-1 (derived by stable transfection of mouse lung epithelial cells with human papillomavirus strain 16 (HPV16) early proteins 6 (E6) and 7 (E7) and activated *H-ras* oncogene) and B16 (melanoma), both of which are resistant to anti-PD-1[10,17]. Anti-PD-1 therapy, when initiated simultaneously (Fig. 1a) with vaccine (Vax + αPD-1), showed synergy in inhibition of tumor growth in the TC-1 model and increased survival of treated animals whereas neither vaccine (Vax) nor anti-PD-1 treatment alone affected tumor growth (Fig. 1b–d and Supplementary Fig. 1a). On the other hand, blockade of PD-1 before antigenic stimulation, by adding one extra dose of anti-PD-1 (Vax + αPD-1 (pre)) into the same schedule (Fig. 1a), fully abrogated the antitumor effects of the combination (Fig. 1b–d and Supplementary Fig. 1a). We found similar results in the B16 tumor model (Fig. 1e–g and Supplementary Fig. 1b). Hence, these results demonstrate that blocking the PD-1 pathway before priming abrogates the antitumor effects of the concomitant combination treatment in two distinct mouse tumor models.

To understand the reason behind the abrogation of the antitumor effects when PD-1 was blocked first, we profiled the T cell infiltrates in the TME using the same schedules outlined earlier. Vaccination resulted in a significant increase in both total and E7-specific $CD8^+$ T cells in the TC-1 model (Fig. 1h,i), which was further increased when anti-PD-1 was given concomitantly with the vaccine. On the other hand, when anti-PD-1 was given before the vaccine, the level of total $CD8^+$ T cells was not changed compared to the vaccine and was significantly lower compared to the Vax + αPD-1 group. We observed a significant decrease in antigen-specific $CD8^+$ T cells after pretreatment with anti-PD-1, resulting in complete elimination of vaccine-induced $E7^+CD8^+$ T cells (Fig. 1i). Anti-PD-1 treatment alone did not show any significant change in the numbers of either $CD8^+$ or antigen-specific $CD8^+$ T cells compared to the untreated control; therefore, this group was not included in the subsequent experiments. Similar results were obtained in the B16 tumor model (Supplementary Fig. 2a,b).

These data demonstrate that PD-1 blockade before antigen priming abrogates the ability of the combination to induce the antigen-specific effector cells and resultant antitumor response.

PD-1 blockade before antigen priming results in increased antigen-specific CD8$^+$ T cell apoptosis and prevents cell activation in the TME

The results described in the previous section suggest that blocking PD-1 before initiating vaccine treatment potentially induces immunologic changes early during the course of treatment that affect the outcome of therapy. Therefore, we analyzed the effect of such treatment on the immune infiltrate 3 d after the priming dose of vaccine given with anti-PD-1 (day 13) (Fig. 2a) and found no significant change in the tumor infiltration of CD8$^+$ T cells (Fig. 2b). However, while the concomitant administration of anti-PD-1 enhanced the E7-specific CD8$^+$ T cell infiltration as early as 3 d after the first vaccination, adding anti-PD-1 before the vaccine led to complete abrogation of this enhancement in the TME (Fig. 2c). In fact, the frequency of E7-specific CD8$^+$ T cells following PD-1 blockade before the vaccine was similar to the untreated control (Fig. 2c). Similar results were obtained in the B16 tumor model (Supplementary Fig. 2c,d). We asked whether the loss in antigen-specific CD8$^+$ T cells in the TME is potentially due to an early induction of apoptosis. We found a significant increase in the apoptotic cell death of total and antigen-specific CD8$^+$ T cells in both TC-1 (Fig. 2d,e) and B16 (Supplementary Fig. 2e–h) models, when anti-PD-1 was started before vaccine compared to the vaccine alone or concomitant treatments. Notably, antigen-specific CD8$^+$ T cells continued to undergo apoptosis on days 13 and 20 (Fig. 2e and Supplementary Fig. 2f,h).

One of the possible causes of apoptosis is the induction of activation-induced cell death (AICD)[19]. Since anti-PD-1 therapy reinvigorates exhausted T cells[20,21] and reverses inhibition of weak TCR signals, leading to CD8$^+$ T cell activation[15,22], we tested the expression of CD40L and interferon-γ (IFN-γ) by CD8$^+$ T cells in the TME as markers of cell activation and functional status[23,24]. Compared to vaccine alone, concurrent treatment resulted in a significant increase in the number of activated CD8$^+$ T cells at day 13 (3 d after antigen priming) (Fig. 2f). Furthermore, concomitant vaccine and anti-PD-1 treatment resulted in increased numbers of IFN-γ-producing cells compared to vaccine alone at day 20 (3 d after antigen boosting) (Fig. 2g). However, the activation status was comparable between the two groups (Fig. 2f). In contrast, the numbers of CD40L$^+$, IFN-γ-producing effector cells decreased significantly when PD-1 was blocked before priming, compared to the concomitant treatment (Fig. 2f,g). Similar results were obtained in the B16 tumor model (Supplementary Fig. 2i–l). These findings, demonstrate that anti-PD-1 given before the vaccine did not induce further activation of T cells; therefore, the observed apoptosis is not due to AICD.

One of the mechanisms of non-AICD-mediated cell death is improper cell activation due to impaired TCR-mediated cell signaling. Hence, we delineated the effect of anti-PD-1 on TCR signaling in CD8$^+$ T cells from Pmel-1 mice (carrying a rearranged TCR transgene (*Vβ13*) specific for the mouse homolog (*pmel-17*) of human *gp100*)[25], activated with cognate gp100 peptide with or without prior anti-PD-1 treatment (Fig. 2h). Src homology region 2 domain-

containing phosphatase-2 (SHP2) phosphorylation inhibits T cell activation through dephosphorylation of tyrosine-protein kinase Lck[26]. Further, PD-1 blockade with simultaneous TCR stimulation releases the brake on cell activation by inhibiting SHP2 phosphorylation[16]. We found that blockade of PD-1 before peptide stimulation led to a significant decrease in phosphorylation of SHP2 while enhancing phosphorylation of Lck and tyrosine-protein kinase ZAP-70 (Zap70) (Fig. 2i–k). Despite further decrease in phospho-SHP2 (Fig. 2i at T3), Lck and Zap70 phosphorylation was significantly decreased with the subsequent addition of anti-PD-1 (Fig. 2j,k at T3). Moreover, the kinase activity of Zap70, as determined by the phosphorylation of linker for activation of T cells family member 1 (LAT) required to trigger downstream TCR signaling, as well as the phosphorylation of the kinase Akt were significantly reduced when cells were treated with anti-PD-1 before peptide stimulation (Fig. 2l,m). These results show that simultaneous treatment with anti-PD-1 and antigen priming induces T cells that maintain their functional status. However, anti-PD-1 given before priming drives T cells into a non-responsive state where LAT and Akt do not get phosphorylated; hence, cells fail to get activated and show effector functions, leading to cell death.

PD-1 blockade before antigenic stimulation generates dysfunctional CD8$^+$ T cells

PD-1$^+$CD38^{hi} CD8$^+$ T cells have been described as a population of dysfunctional cells that fail to respond to antigenic stimulation and do not elicit effector functions[18], similar to the characteristics of cells generated after PD-1 blockade before antigen priming as described earlier. Therefore, we determined the expression of CD38 on PD-1$^+$CD8$^+$ T cells following concomitant or prior anti-PD-1 treatment with respect to vaccine in TC-1 tumor-bearing mice (Supplementary Fig. 3a). Anti-PD-1 treatment before antigenic priming led to a significant increase in the expression of CD38 (mean fluorescence intensity (MFI)) as well as in the number of PD-1$^+$CD38^{hi} total and antigen-specific CD8$^+$ T cells in comparison to vaccine treatment (Fig. 3a,b and Supplementary Fig. 3b). However, when anti-PD-1 was given simultaneously with vaccine, a significant decrease in the expression of CD38 (MFI) and number of PD-1$^+$CD38^{hi} total and antigen-specific CD8$^+$ T cells was observed (Fig. 3a,b). Similar results were observed in B16 tumor-bearing mice (Fig. 3c,d).

We next determined the functionality of these cells generated after various treatments and found that PD-1$^+$CD38^{hi} cells induced as a result of anti-PD-1 pretreatment were dysfunctional since they failed to upregulate CD40L and did not produce IFN-γ after antigenic restimulation (Fig. 4a,b). On the other hand, most cells generated by simultaneous anti-PD-1 and vaccine treatment had low expression of CD38 on PD-1$^+$CD8$^+$ T cells (PD-1$^+$CD38^{lo} T cells) (Fig. 3a,b) and were highly functional as evident by upregulated CD40L and IFN-γ production (Fig. 4a,b). Moreover, dysfunctional PD-1$^+$CD38^{hi} CD8$^+$ T cells induced after anti-PD-1 was administered before vaccine also showed significantly higher apoptosis in both total and antigen-specific CD8$^+$ T cells (Fig. 4c,d). Notably, we found similar results in the B16 tumor model (Supplementary Fig. 4a–d). These data clearly indicate that blocking PD-1 signaling before antigenic stimulation drives the antigen-specific CD8$^+$ T cells into a dysfunctional state early (day 13) during the course of antigenic stimulation while they remained functional when PD-1 signaling was blocked concomitant to TCR stimulation.

Since $CD8^+$ T cells did not become activated, which is necessary for memory generation, we reasoned that anti-PD-1 treatment before antigenic stimulation would result in impaired immune memory generation. Indeed, we found that mice that were treated with anti-PD-1 before vaccine treatment had significantly lower central ($CD62L^+CD44^+$) (Fig. 4e) and effector ($CD62L^-CD44^+$) (Fig. 4f) memory than vaccine alone or concomitant (Vax + αPD-1) treatment groups.

Depletion of $PD\text{-}1^+CD38^{hi}$ $CD8^+$ T cells results in a strong antitumor response

As shown earlier, PD-1 blockade before antigenic stimulation generated dysfunctional $PD\text{-}1^+CD38^+$ $CD8^+$ T cells, resulting in increased cell death and reduced memory. However, to establish if these cells are the cause of the adverse antitumor effects seen after anti-PD-1 therapy, we performed adoptive cell therapy (ACT) experiment in *Rag1*$^{-/-}$ mice whereby we transferred either a total activated $CD8^+$ T cell culture or a $PD\text{-}1^+CD38^+$-depleted $CD8^+$ T cell culture (Fig. 5a), which accounted for approximately 30% of the total cell culture. We found that depletion of $PD\text{-}1^+CD38^+$ T cells enhanced the antitumor therapeutic effects of activated $CD8^+$ T cells (Fig. 5a and Supplementary Fig. 5a), thus confirming that the $PD\text{-}1^+CD38^+$ T cells were the dysfunctional cells. Next, to establish the mechanistic link between CD38 expression and dysfunction of $CD8^+$ T cells, we flow-sorted $PD\text{-}1^+CD38^+$ T cells, knocked down CD38 using small interfering RNA (Supplementary Fig. 5b) and estimated the ability of these cells to proliferate and demonstrate effector functions (Fig. 5b). We found that on CD38 knockdown (Fig. 5c), $PD\text{-}1^+CD38^+$ T cells regained their ability to proliferate, activate and express effector molecules (Fig. 5d). Thus, these data show that CD38 is not merely a marker of cell dysfunctionality but serves a mechanistic role in rendering $CD8^+$ T cells dysfunctional.

PD-1 blockade on suboptimally primed $CD8^+$ T cells induces dysfunctional $PD\text{-}1^+CD38^{hi}$ $CD8^+$ T cells both in vivo and in vitro

Since treatment with anti-PD-1 before proper priming resulted in the induction of dysfunctional cells, we next tested whether treatment with anti-PD-1 alone leads to the generation of these dysfunctional cells. Accordingly, the phenotype of $CD8^+$ T cells was analyzed in the TME 3 d after administration of a single dose of anti-PD-1 (day 10) in TC-1 tumor-bearing mice (Fig. 6a). We found that anti-PD-1 significantly increased the expression of CD38 (MFI) on $PD\text{-}1^+CD8^+$ T cells, resulting in a significant increase in the number of $PD\text{-}1^+CD38^{hi}$ $CD8^+$ T cells (Fig. 6b). Furthermore, compared to the untreated control, PD-1 blockade resulted in a 2–3 times increase in annexin V expression in both total and $PD\text{-}1^+CD38^{hi}$ $CD8^+$ T cells, despite the lack of change in the numbers of total $CD8^+$ T cells in the TME (Fig. 6c). Together with similar findings in the B16 melanoma model (Fig. 6d,e), these results suggest that blocking the PD-1 or PD-L1 pathway without proper priming predisposes $CD8^+$ T cells toward dysfunction and apoptosis-mediated cell death. To further confirm these findings, we used ovalbumin (OVA) peptide-specific TCR-transgenic OT I mice to compare the level of induction of dysfunctional $PD\text{-}1^+CD38^{hi}$ cells in $CD8^+$ T cells stimulated either with high- (OVA; optimum priming) or low-affinity antigen (OVA-V; suboptimal priming)[27] with or without anti-PD-1 treatment (Fig. 7a). TCR stimulation with low-affinity OVA-V antigen led to a significantly lower level of cell activation (CD40L expression and IFN-γ production) compared to stimulation with high-affinity OVA antigen

(Fig. 7b,c). We found that the expression of CD38 in PD-1^{+}CD8^{+} T cells (Fig. 7d) and the number of PD-1^{+}CD38^{hi} CD8^{+} T cells (Fig. 7e) after suboptimal OVA-V stimulation were significantly higher compared to OVA stimulation and showed increased apoptosis (Fig. 7f). Furthermore, treatment of OVA-V-stimulated CD8^{+} T cells with anti-PD-1 resulted in an increase in the number of PD-1^{+}CD38^{hi} cells (Fig. 7e). In contrast, treatment of OVA-stimulated CD8^{+} T cells with anti-PD-1 showed no change in the number of PD-1^{+}CD38^{hi} cells (Fig. 7e). However, blocking PD-1 before priming with OVA also resulted in a significant increase in the number of dysfunctional T cells (Fig. 7e). These PD-1^{+}CD38^{hi} T cells underwent apoptosis-mediated cell death (Fig. 7f).

This in vitro experiment further indicated that when CD8^{+} T cells are suboptimally primed they have a tendency to develop into a dysfunctional phenotype that is exacerbated on treatment with PD-1 blockade. Also, these data indicate that blocking PD-1 before CD8^{+} T cell activation even with a strong antigen leads to the development of the dysfunctional CD8^{+} T cell phenotype. To further test this in vivo, we inoculated mice with TC-1 tumor in the presence or absence of concomitant priming with gp100 peptide (day 0) followed by anti-PD-1 administration at day 7 (Fig. 7g). We used a non-cognate tumor vaccine to mitigate the effects of the tumor-specific immune response. We found that in suboptimally primed TC-1 tumor-bearing mice, anti-PD-1 treatment significantly induced PD-1^{+}CD38^{hi} T cells (Fig. 7h). On the other hand, priming mice with gp100 at the time of tumor inoculation prevented the induction of these dysfunctional cells, which were further reduced on anti-PD-1 treatment compared to both untreated and anti-PD-1-treated groups (Fig. 7h). Although gp100 alone prevented the induction of these dysfunctional cells, their function was only increased when anti-PD-1 was given subsequent to priming with gp100 peptide (Fig. 7i), demonstrating that optimal priming of cells is essential to enhance the anti-PD-1-mediated functionality of cells. Together, these results demonstrate that the suboptimal priming of CD8^{+} T cells induces higher numbers of dysfunctional PD-1^{+}CD38^{hi} CD8^{+} T cells and their frequency further increases on anti-PD-1 therapy, potentially leading to therapeutic failure. Since in most tumors T cells are suboptimally primed[28,29], our mouse data demonstrate the importance of appropriately primed T cells in responding to anti-PD-1 treatment.

Number of PD-1^{+}CD38^{hi} CD8^{+} T cells in tumors correlate with the anti-PD-1 therapeutic response in patients

Based on the data outlined earlier, we next tested whether PD-1^{+}CD38^{hi} CD8^{+} T cells are also important in predicting response to PD-1 blockade in humans. We evaluated the levels of PD-1^{+}CD38^{+} CD8^{+} T cells using single-cell RNA sequencing of CD45^{+} immune cells from freshly dissociated tumor biopsies from patients (n = 32) treated with either anti-PD-1 (n = 24) or anti-PD-1 + anti-cytotoxic T-lymphocyte protein 4 (CTLA-4) (n = 8) antibodies as described earlier[30]. Biopsies (n = 48 from 32 patients) were from baseline or posttreatment metastatic melanoma patients. Analysis of post-therapy non-responding tumor lesions (n = 21) showed that the fraction of PD-1^{+}CD38^{+} CD8^{+} T cells was significantly higher compared to the fraction in responder lesions (n = 8) ($P \leq 0.01$) (Fig. 8a). Based on an a priori determination of the threshold percentage of PD-1^{+}CD38^{+} CD8^{+} T cells that was confirmed by receiver operating characteristics (ROC) analysis to best predict responders

versus non-responders (Supplementary Fig. 6a), we found that 100% of non-responding patients had >4% PD-1^{+}CD38^{+} cells in the CD8^{+} population in the TME compared to only 25% of responding patients ($P \leq 0.0001$) (Fig. 8a), with a positive predictive value (PPV) of 0.913, negative predictive value (NPV) of 1.0, sensitivity and specificity of 1.0 and 0.75, respectively and area under the ROC curve (AUC) of 0.887 (Supplementary Fig. 6a), indicating a strong potential for the PD-1^{+}CD38^{+} CD8^{+} T cell fraction in the TME to serve as a biomarker for post-therapeutic outcome.

Based on these post-therapy patient findings, and since most of the patients have suboptimally primed CD8^{+} T cells in the TME before therapy[31], potentially leading to the development of the dysfunctional PD-1^{+}CD38^{hi} CD8^{+} T cell phenotype (Fig. 7d,e), we tested whether the higher frequency of these cells also exists before anti-PD-1 therapy and can predict outcome. Indeed, we found that the fraction of PD-1^{+}CD38^{+} CD8^{+} T cells in the tumor samples obtained before therapy ($n = 19$) from non-responders ($n = 10$) was significantly higher compared to responders ($n = 9$; $P \leq 0.01$) and that 25% of the CD8^{+} T cells expressed PD-1^{+}CD38^{+} in non-responders versus <5% in responders (Fig. 8b). Furthermore, we found that 80% of non-responding patients had >10% PD-1^{+}CD38^{+} T cells in the CD8^{+} population, compared to only 33% of responding patients ($P = 0.023$; Fig. 8b). An AUC of 0.833 with a PPV of 0.727 and NPV of 0.75 suggests that the PD-1^{+}CD38^{+} CD8^{+} T cell fraction in the TME can serve as a potential predictive biomarker of therapeutic response to anti-PD-1 (Fig. 8b and Supplementary Fig. 6b). We found that similar numbers of CD8^{+} T cells infiltrated non-responding and responding tumor lesions with higher absolute numbers of PD-1^{+}CD38^{+} CD8^{+} T cells in non-responding lesions (Fig. 8c). These results confirm that the differences in the fraction of PD-1^{+}CD38^{+} CD8^{+} T cells in non-responding versus responding tumor lesions are not simply due to higher numbers of total CD8^{+} T cells in the TME.

Since obtaining tumor biopsies either at baseline or post-therapy may be a major hindrance, we asked whether the PD-1^{+}CD38^{+} CD8^{+} T cell fraction can also be measured in peripheral blood mononuclear cells (PBMCs). We tested the CD38^{+} fraction of PD-1^{+}CD8^{+} T cells in PBMCs obtained post-therapy from responders and non-responders at 3 and 9 weeks from another clinical trial of anti-PD-1 therapy in advanced melanoma patients. We found that the CD38^{+} fraction of PD-1^{+}CD8^{+} T cells showed more than a 5% decline at 9 weeks compared with 3 weeks in 13 out of 14 responding patients (93%), while most non-responding patients showed stabilization or an increase in the CD38^{+} fraction in PD-1^{+}CD8^{+} T cells (7 of 9 patients (78%); in addition to these 9 patients, data for 2 patients are shown at 6 weeks since the 9 week values were not available; $P \leq 0.001$, AUC = 0.864, PPV = 0.9, NPV = 0.867, sensitivity = 0.818 and specificity = 0.929) (Fig. 8d and Supplementary Fig. 6c). This indicates that the CD38^{+} fraction of PD-1^{+}CD8^{+} T cells in PBMCs merits further investigation as an early pharmacodynamic biomarker for anti-PD-1 therapy.

Discussion

In the present study, we show that the status of CD8^{+} T cell priming is a major contributor to anti-PD-1 therapeutic resistance. PD-1 blockade under unprimed or suboptimally primed CD8^{+} T cell conditions induced a dysfunctional PD-1^{+}CD38^{hi} phenotype, rendering mice

resistant to further anti-PD-1 therapy. On the other hand, proper antigen priming prevented the anti-PD-1-mediated induction of these dysfunctional cells, reversing the anti-PD-1 resistance. Furthermore, we found that tumors generating suboptimally primed $CD8^+$ T cells develop dysfunctional cells that get further increased with PD-1 blockade. The induction of dysfunctional $CD8^+$ T cells by these tumors could be reversed if mice were optimally primed at the time of tumor implantation, even with an irrelevant antigen, preventing anti-PD-1 resistance. Accordingly, we established that the $CD8^+$ T cell priming conditions are the crucial determinant of anti-PD-1 therapeutic outcome. These data provide a potential explanation to some of the outcomes we see in the clinical setting since most cancer patients present with suboptimally primed $CD8^+$ T cells[28,29]. Our findings also explain the preferentially superior response rates to anti-PD-1 therapy in patients with higher mutational burden (expression of neoantigens, leading to appropriate T cell priming)[32,33] and tumors with high T cell infiltration (‘hot tumors’), such as desmoplastic melanoma, Merkel cell carcinoma and microsatellite instability^{high} tumors[33–35]. These observations strongly suggest that anti-PD-1-mediated resistance can potentially be prevented by concomitant therapies that increase the antigenicity of the tumor. Furthermore, the data also show that the sequence of anti-PD-1 and vaccine combination is important for therapeutic success, since blocking anti-PD-1 before proper priming leads to the development of resistance to the vaccine effect. This is an important finding since many clinical trials combining vaccine with anti-PD-1 start with PD-1 blockade because of the time required to prepare tumor-specific vaccines.

For proper functioning of $CD8^+$ T cells, the crosstalk between PD-1 and TCR signaling is an important determinant[16,36]. Indeed, we found that interaction of PD-1 and TCR-mediated signaling turns errant after PD-1 blockade in suboptimal T cell priming conditions. Upregulation of phospho-Lck and phospho-Zap70 prepares cells for activation by phosphorylating the downstream TCR kinases LAT and Akt[37,38]. However, despite activation of both Lck and Zap70, PD-1 blockade before antigen stimulation led to a decrease in the phosphorylation of LAT and Akt. Although the reason for this aberrant effect is currently not clear, it could be because of the failure of TCR complex clustering due to the absence of proper antigen engagement[39], in turn preventing the activation of LAT and Akt.

It has been shown that anti-PD-1 can reinvigorate exhausted $CD8^+$ T cells[40,41]. However, this is dependent on the initial cell activation status where anti-PD-1 resurrects the cells that have been exhausted after strong chronic antigenic stimulation. In contrast, the dysfunctional PD-1^+CD38^{hi} phenotype is generated when PD-1 is blocked before proper antigenic stimulation, inducing a terminally dysfunctional phenotype that does not show any effector functions or memory generation; cells undergo apoptosis after antigenic rechallenge.

Through depletion experiments, we found that PD-1^+CD38^{hi} $CD8^+$ T cells are not merely an indicator for anti-PD-1 therapeutic failure, but rather directly contribute to the failure. This may be due to the dominance of these dysfunctional cells among tumor antigen-specific $CD8^+$ T cells. Alternatively, PD-1^+CD38$^+$ T cells may actively inhibit tumor-reactive effector cells, possibly by depleting essential nutrients[42]. This, in turn, leads to lack of activation and induction of apoptosis in a substantial fraction of $CD8^+$ T cells[43]. Although further delineation of the underlying mechanisms responsible for the unresponsiveness of

PD-1^{+}CD38^{hi} CD8^{+} T cells to anti-PD-1 are needed, it is clear that targeting PD-1^{+}CD38^{hi} CD8^{+} T cells may prevent the induction of resistance to anti-PD-1 therapy. Furthermore, the mechanism of CD38 induction is still not clear; its association with the dysfunctional phenotype is unequivocally demonstrated by the regaining of effector functions when CD38 is silenced by genetic knockdown. Therefore, as shown earlier, while PD-1 expression reflects T cell reactivity to antigen exposure[44,45], we believe that the associated expression of CD38 reflects the dysfunctionality of these CD8^{+} T cells.

Indeed, we found that this is very relevant to humans where patients who fail anti-PD-1 therapy have high numbers of dysfunctional PD-1^{+}CD38^{hi} CD8^{+} T cells in the TME, compared to responding patients. Hence, PD-1^{+}CD38^{hi} CD8^{+} T cells can serve as a potential predictive biomarker for anti-PD-1 therapy. Furthermore, we also showed that in non-responding patients, the number of PD-1^{+}CD38^{hi} CD8^{+} T cells remains stable or rises during therapy in PBMCs, in contrast to the decreasing level in responding patients. Accordingly, PD-1^{+}CD38^{hi} CD8^{+} T cells can also be used as an early marker for response. Currently, there are only a few biomarkers that are available for predicting response to anti-PD-1 in a binary manner[46]. PD-L1 expression on tumors has been used as a predictor of response to anti-PD-1 therapy[46]. However, limitations such as the robust responses in patients with low PD-L1 expression on tumors and its variable expression over the course of tumor progression restrict its use[47,48]. Given the difficulty in obtaining serial tumor samples, correlation of high numbers of these cells in the blood of non-responding patients provides an opportunity in serial monitoring of anti-PD-1 immunotherapy. The signatures of T cell dysfunction and exclusion have been shown to predict cancer immunotherapy response with an AUC of approximately 0.8 (ref. [49]). However, our study provides an easier and cost-effective prediction method with a very high predictive power of PD-1^{+}CD38^{hi} CD8^{+} T cells for anti-PD-1 therapy with an AUC >0.8. We recognize that these statistics and observations are from a limited number of patients and are done retrospectively. Future prospective studies done in a large pool of patients would be helpful in better establishing the predictive efficiency of these dysfunctional cells.

Our study has several implications. First, simultaneous blockade of PD-1 along with TCR stimulation using cancer vaccine results in reversal of resistance to anti-PD-1 therapy. This suggests that resistance to anti-PD-1 therapy can be prevented by simultaneous treatment with cell-activating therapies such as vaccination, immune stimulatory antibodies or radiation therapy. Second, sequencing of vaccine and anti-PD-1 is crucial in determining the therapeutic outcomes that would affect several ongoing clinical trials[50]. Third, PD-1 blockade of suboptimally primed CD8^{+} T cells results in the generation of a dysfunctional PD-1^{+}CD38^{hi} phenotype that is refractory to further stimulation. Fourth, the high expression of CD38 directly contributes to the dysfunctionality of CD8^{+} T cells, and the PD-1^{+}CD38^{hi} phenotype of CD8^{+} T cells can be a predictive and therapeutic biomarker of anti-PD-1 treatment as well as for selecting patients that would benefit from anti-PD-1 therapy.

Methods

Human samples and processing

Tumor samples—The expression of CD38 and PD-1 in $CD8^+$ T cells (Fig. 8a–c) is an earlier published dataset from 48 tumor samples from a cohort of 32 metastatic melanoma patients treated with either anti-PD-1 ($n = 24$ patients; $n = 32$ tumor biopsies) or anti-PD-1 + anti-CTLA-4 ($n = 8$ patients; $n = 16$ tumor biopsies)[30]. Biopsies were taken either at baseline ($n = 19$) or posttreatment ($n = 29$) and were not matched for individual patients. Patient responses were evaluated using the RECIST criteria[51]. For this analysis we focused on individual tumor samples and classified them into two categories: responding lesions (regression; $n = 17$, including complete response and partial response samples, at baseline $n = 9$ and posttreatment $n = 8$) and non-responding lesions (progression; $n = 31$, including stable disease and progressive disease samples, at baseline $n = 10$ and posttreatment $n = 21$) based on radiological tumor assessments. Fresh tumor biopsies were dissociated using the human Tumor Dissociation Kit (catalog no. 130–095-929; Miltenyi Biotec), sorted using a BD Fusion instrument into 96-well plates (catalog no. 951020401; Eppendorf) containing 10 μl of lysis buffer (TCL buffer, catalog no. 1031576, QIAGEN; containing 1% β-mercaptoethanol) using the following anti-human antibodies (all BioLegend): TruStain FcX (catalog no. 422302); Zombie violet (catalog no. 423113); CD45-PE (catalog no. 304008); CD3-APC (catalog no. 300412); CD235a-APC/Cy7 (catalog no. 349116); CD8-Brilliant Violet 650 (catalog no. 301041); and HLA-A,B,C-FITC (catalog no. 311426)[30]. Immediately after sorting, the plates were stored at −80°C until processing. Libraries were generated for $CD45^+$ cells using a modified version of the full-length Smart-Seq2 protocol as described recently[52], resulting in a median of approximately 1.4 million paired-end reads and a median of 2,588 genes detected per cell. Sequencing was performed on a NextSeq 500 sequencer (Illumina). A total of 16,291 $CD45^+$ cells or 6,350 $CD8^+$ T cells that passed quality control were used for downstream analysis. For each sample, we computed the fraction of $CD38^+PD\text{-}1^+$ cells out of $CD8^+$ T cells. A cutoff of $\log^2(TPM + 1) \geq 2$ was used to define a gene as expressed in each single cell.

PBMC samples—Human PBMC samples from stage IV melanoma patients (at baseline and up to 3 on-treatment (pembrolizumab therapy) visits (collected approximately every 3 weeks)) from 15 responders and 16 non-responders were from a previously reported clinical trial (NCT01295827)[14]. PBMCs were thawed and stained with a LIVE/DEAD fixable near-IR dead cell stain kit (Invitrogen; catalog no. L10119) and a cocktail of antibodies to the following surface markers: CD8-Qdot605 (clone 3B5, catalog no. Q10009; Invitrogen); PD-1-PE (clone MIH4, catalog no. 557946; BD Biosciences); and CD38-PerCP-Cyanine 5.5 (clone HIT2, catalog no. 303521; BioLegend)[14]. Control stains were also performed on each sample using isotype control antibodies for PD-1 and CD38 to determine marker positivity. Stained cells were acquired on an LSRFortessa (BD Biosciences) and analyzed with the FlowJo software (FlowJo, LLC).

Ethical approval of the study protocols—The cohorts were not collected as part of this study. However, the Memorial Sloan Kettering Cancer Center (MSKCC), Dana-Farber/Harvard Cancer Center and University of Texas MD Anderson Cancer Center approved the

study protocols (MSKCC, protocol 00–144; Dana-Farber/Harvard Cancer Center Institutional Review Board, DF/HCC protocol 11–181; and University of Texas MD Anderson Cancer Center, IRB LAB00–063 and 2012–0846).

The studies were performed in accordance with protocols, good clinical practice standards and the Declaration of Helsinki; protocols and all amendments were approved by the appropriate institutional review board or ethics body at each institution. All patients provided written informed consent.

Mice

C57BL/6J and *Rag1*$^{-/-}$ female mice, 4–6 weeks old, were purchased from The Jackson Laboratory and housed under pathogen-free conditions. For the in vitro experiments, Pmel-1 mice (B6.Cg-Thy1^{a}/Cy Tg (TcraTcrb)8Rest/J) that carry a rearranged TCR transgene (*Vβ13*) specific for the mouse homolog (*pmel-17*) of human *gp100* (ref. [53]) and OT I mice (C57BL/6-Tg(TcraTcrb)1100Mjb/Crl) that have transgenic TCR on CD8^{+} T cells specific for OVA residues 257–264 in the context of H-2Kb were used. All procedures were carried out in accordance with approved Institutional Animal Care and Use Committee animal protocols at Augusta University and Georgetown University. Pmel-1 and OT I mice were bred in-house and maintained under specific pathogen-free conditions.

Tumor cell lines

TC-1 cells that were derived by stable transfection of mouse lung epithelial cells with human papilloma virus 16 (HPV16) early proteins E6 and E7 and activated *H-ras* oncogene were obtained from T-C. Wu (Johns Hopkins University)[54]. The B16 (melanoma) tumor cell line expressing gp100 was obtained from the American Type Culture Collection. Cells were grown in Roswell Park Memorial Institute (RPMI) 1640 growth medium supplemented with 10% fetal bovine serum (FBS), 2 mM L-glutamine, penicillin (100 U ml^{-1}) and streptomycin (100 μg ml^{-1}) at 37 °C with 5% CO_2 and maintained at a confluence of 70–80%. The cells were routinely tested for the absence of *Mycoplasma* by applying PCR at the Georgia Cancer Center, Augusta University. All tests were negative.

Vaccines

The cytotoxic T lymphocyte epitope from HPV16 E7$_{49–57}$ (9-amino acid peptide, RAHYNIVTF, 100 μg per mouse) from Celtek Bioscience was used for the TC-1 tumor model. For the B16 tumor model, gp100$_{25–33}$ peptide vaccine was used. The gp100$_{25–33}$ enneamer peptide (KVPRNQDWL) was purchased from AnaSpec and administered at 100 μg per mouse[25]. Both vaccines were used mixed with PADRE (aK-Cha-VAAWTLKAAa, where ‘a’ is D-alanine and ‘Cha’ is L-cyclohexylalanine), a small triadecamer non-natural pan HLA-DR binding sequence that is a potent T cell epitope (T helper epitope, 20 μg per mouse; Celtek Bioscience) and QuilA (adjuvant, 10 μg per mouse; Brenntag). Respective vaccines were administered subcutaneously (s.c.) every 7 d in TC-1 or B16 tumor-bearing mice. For the therapeutic experiments, mice were vaccinated three times, with an interval of 1 week between vaccinations; for the immune response experiments, mice were vaccinated twice.

Various cell types were activated with their respective cognate peptides. The $gp100_{25–33}$ enneamer peptide (KVPRNQDWL) was used for in vitro activation of magnetically enriched $CD8^+$ T cells from the spleens of Pmel-1 mice[55] while $CD8^+$ T cells from OT I mice were activated with $OVA_{257–264}$ (SIINFEKL). In some experiments, a low-affinity variant of $OVA_{257–264}$, termed OVA-V (SIIGFEKL) was used to activate OT I $CD8^+$ T cells. The purity of the enriched cells was >90%.

Antibodies and reagents

Purified anti-mouse anti-PD-1 (RMP1–14 clone, Rat IgG2a) was obtained from MedImmune. The Live/Dead Fixable Near-IR Dead Cell Stain Kit (catalog no. L34976) and CellTrace Violet Cell Proliferation Kit (catalog no. C34557) were obtained from Thermo Fisher Scientific. The fluorochrome-labeled anti-mouse antibodies used for flow cytometry measurements were V450-CD45 (1:200, clone 30-F11, catalog no. 103125; eBioscience); TxRd-CD3 (1:200, clone 145–2c11, catalog no. 562286; BD Biosciences); Alexa Fluor 700-CD8a (1:200, clone 53–6.7, catalog no. 557959; BD Biosciences); PE-Annexin V (1:200, catalog no. 556421; BD Biosciences); PE-CD40L (1:20, clone MR1, catalog no. 553658; BD Biosciences), FITC-IFN-γ (1:100, clone xmg1.2 catalog no. 557724; BD Biosciences), Alexa Fluor 700-CD62L (1:200, clone MEL-14, catalog no. 560517; BD Biosciences); FITC-CD44 (1:200, clone IM7, catalog no. 553133; BD Biosciences); Alexa Fluor 700-CD38 (1:200, clone 90, catalog no. 56–0381-82; Invitrogen); PE-PD-1 (1:200, clone 29 F.1A12, catalog no. 135206; BioLegend); APC-Ki-67 (1:200, clone SolA15, catalog no. 17–5698-82; Invitrogen); Alexa Fluor 647-p-SHP2 (pY542) (1:10, clone L99–921, catalog no. 560390; BD Biosciences); PE-phospho-Akt (pS473) (1:10, clone M89–61, catalog no. 560378; BD Biosciences); PerCP-eFluor710-p-Lck (Tyr505) (1:10, clone SRRCHA, catalog no. 46–9076-42; Invitrogen); PE-p-Zap70 (Y319, Y352) (1:10, clone 17 A/P-ZAP70 (RUO), catalog no. 557881; BD Biosciences); and AF647-p-LAT (Tyr200) (1:10, polyclonal, catalog no. bs-10128R-A647; Bioss Antibodies). FITC-E7 (1:50, catalog no. JA2195-FITC) and APC-gp100 (1:50, catalog no. WB2158-APC) dextramers were obtained from Immudex. $CD8^+$ enrichment kits (Miltenyi Biotec) were used according to the manufacturer's instructions. Anti-CD38 antibody for the immunoblot was obtained from Proteintech (1:100, clone 3C6G4, catalog no. 60006–1-Ig) while anti-β-actin (anti-mouse) antibody was purchased from Sigma (1:1,000, clone AC-15, catalog no. A5441). Rabbit anti-mouse horseradish peroxidase (HRP)-labeled secondary antibodies were obtained from Cell Signaling Technology.

Tumor implantation, immunization, antibody treatment and tumor volume measurement

In the therapeutic experiments, tumors were implanted in C57BL/6J mice by injecting either 7×10^4 TC-1 or 0.1×10^6 B16 tumor cells per mouse s.c. into the right flank at day 0. When tumors measured approximately 5–6 mm in diameter, mice from the appropriate groups (10–20 mice per group) were injected with vaccine (s.c., total of 3 doses, 1 week apart). Anti-PD-1 was administered intraperitoneally (i.p.) twice weekly throughout the experiment at a dose of 1 mg kg^{-1} for TC-1 and 5 mg kg^{-1} for B16 tumor models beginning either 3 d before (αPD-1 (pre)) or at the day of vaccination. Tumors were measured every 3–4 d using a digital Vernier caliper; tumor volume was calculated using the formula $V = (L \times W^2)/2$, where V is tumor volume, L is the length of the tumor (longer diameter) and W is the width

of the tumor (shorter diameter). Mice were monitored for tumor growth and survival. Mice were killed when tumor volume reached 1.5 cm^3.

For the immune response experiments, TC-1 or B16 tumor-bearing mice were treated according to the same schedule as for the therapy experiment, except only two doses of weekly vaccines were given. Tumor samples were collected at various time points: day 10, that is, 3 d after anti-PD-1 treatment; day 13, that is, 3 d after first vaccination; and day 20, that is, 3 d after the second vaccination. Samples were processed with the gentleMACS dissociator and the solid tumor homogenization protocol, as suggested by the manufacturer (Miltenyi Biotec). Each experiment was repeated at least twice.

In a separate experiment, C57BL/6 mice were implanted with TC-1 tumor, and gp100 vaccine was administered at the same time (day 0) followed by anti-PD-1 at day 7. Three days after anti-PD-1 treatment (day 10), tumor samples were collected followed by flow cytometry analysis of the immune repertoire in the tumors.

Flow cytometry analysis of tumor-infiltrating lymphocytes and apoptosis

For the flow cytometry analysis of tumor-infiltrating lymphocytes, $1–2 \times 10^6$ cells per sample per time point were stained with the LIVE/DEAD stain (Invitrogen) followed by fixation and permeabilization. For IFN-γ staining, the BD Biosciences Cytofix/Cytoperm (catalog no. 51–2090KZ) and BD Biosciences Perm/Wash (catalog no. 51–2091KZ) buffer sets were used according to the manufacturer's instructions. Data acquisition was performed on FACSCalibur or LSRFortessa platform (BD Biosciences). Results were analyzed with the FlowJo software. Total numbers of $CD3^+$, $CD8^+$, $CD8^+E7^+$, annexin V^+, $CD40L^+$, IFN-γ^+, $CD62L^+$, $CD44^+$, $CD38^+$ and PD-1^+ cells were analyzed within the $CD45^+$ hematopoietic cell population and represented in 1×10^6 live cells in tumors or the respective populations, as shown in the figures. In addition, expression of CD38 (MFI) was estimated on the PD-1^+CD8^+ T cell population.

To determine apoptosis, freshly collected tumor tissues from variously treated mice were processed into single-cell suspensions and stained for CD8, E7CD8, PD-1, CD38 and annexin V according to the manufacturer's protocol (BD Biosciences) and were acquired by fluorescence-activated cell sorting (FACS).

Cell activation

For in vitro activation, magnetically enriched (Miltenyi Biotec) $CD8^+$ T cells (>95% purity) from Pmel-1 mice were cultured in T cell medium containing RPMI 1640 (Lonza) supplemented with 10% FBS, penicillin (100 U ml^{-1}), streptomycin (100 mg ml^{-1}), 0.1% β-mercaptoethanol and either interleukin-2 (IL-2, 100 U ml^{-1}) (PeproTech) or anti-PD-1 + IL-2 (clone- RMP1–14, 25 μg ml^{-1}; MedImmune) at 37 °C, 5% CO_2. Twenty-four hours later, cells were collected for flow cytometry analyses (T1) or cells were further cultured for 24 h following the addition of anti-PD-1 (25 μg ml^{-1}), $gp100_{25–33}$ peptide (0.2 μM ml^{-1}) and IL-2 for 24 h. At the end of incubation, cells were again collected for flow cytometry analyses (T2). Finally, cells were cultured for 48 h following the addition of anti-PD-1 (25 μg ml^{-1}) + IL-2 and collected for flow cytometry analyses (T3). Collected cells were analyzed for expression of phosphorylated SHP2, Lck, Zap70, LAT and Akt by FACS.

To activate OT I T cells, magnetically purified (>90%) $CD8^+$ T cells were incubated either with IL-2 (100 U ml^{-1}) or IL-2 + αPD-1 (25 μg ml^{-1}) for 24 h followed by the addition of OVA or OVA-V (1 μg ml^{-1}) with αPD-1 and IL-2 for an additional 24 h, as shown in the schematic in Fig. 7a. At the end of incubation, cells were collected and analyzed by FACS for the expression of PD-1, CD38, CD40L, IFN-γ and annexin V.

To analyze the production of IFN-γ by $CD8^+$ T cells in the TME, $CD8^+$ T cells from freshly acquired tumor samples from variously treated mice were plated at a density of 2×10^6 cells per well in a 48-well plate and incubated in T cell medium containing 50 ng ml^{-1} of phorbol 12-myristate 13-acetate (catalog no. P1585; Sigma-Aldrich), 750 ng ml^{-1} of ionomycin and 10 μg ml^{-1} of brefeldin (catalog no. B5936–200UL; Sigma-Aldrich). Cells were incubated for 4 h at 37 °C with 5% CO_2 followed by FACS staining to detect IFN-γ and other cell markers.

CD38 knockdown

To induce high levels of CD38, Pmel $CD8^+$ T cells were treated overnight with αPD-1 followed by overnight activation with gp100 + αPD-1. PD-$1^+$$CD38^+$ $CD8^+$ T cells were collected by FACS sorting. Sorted PD-$1^+$$CD38^+$ cells were rested for 2–3 h in T cell medium at 37 °C. The rested PD-$1^+$$CD38^+$ cells (50,000 well 200μl^{-1}) were suspended in T cell medium containing 1% FBS. CD38-siRNA (catalog no. AM16708; Ambion) or control (scrambled) RNA (catalog no. AM4611; Ambion) was prepared using Lipofectamine RNAiMAX Reagent and OPTI-MEM (both from Thermo Fisher Scientific) according to the manufacturer's recommendations. siRNA was used at a final concentration of 10 μM. After incubation overnight, cells from the appropriate treatment (scrambled RNA versus siRNA) were tested for CD38 expression by FACS and immunoblot analysis. In the respective treated cells, gp100 + αPD-1 was added as described earlier followed by incubation overnight at 37 °C. The next day, siRNA-treated cells were analyzed for their ability to proliferate (Ki-67), become activated (CD40L) and show effector functions (IFN-γ) by FACS analysis.

Immunoblot analysis

Pmel-1 $CD8^+$ T cells collected as described earlier were treated with cell lysis buffer (radioimmunoprecipitation assay buffer + 1% phosphatase inhibitor + 1% protease inhibitor) to prepare the cell lysates. Protein concentrations in the cell lysates were determined by Pierce BCA Protein Assay Kit (Thermo Fisher Scientific); 20–30 μg protein was loaded onto Novex 4–20% Tris-Glycine Mini Gels (Thermo Fisher Scientific) followed by transfer onto nitrocellulose membranes. Membranes were blocked with 3% BSA in Tris-buffer followed by overnight probing of the proteins with antibodies directed against mouse CD38. Blots were developed with rabbit anti-mouse HRP-labeled secondary antibodies.

ACT

$CD8^+$ T cells from Pmel-1 mice were pretreated overnight with αPD-1 and activated overnight with gp100 + αPD-1. This was followed by adoptive transfer of either total, activated $CD8^+$ T cell culture or total culture minus PD-$1^+$$CD38^+$ T cells into *Rag1*$^{-/-}$ mice bearing 7-day-old B16 tumors. One million cells were transferred into each mouse in each

treatment group. Mice were vaccinated with gp100 vaccine, 1 and 7 d after cell transfer. Mice were observed for tumor growth and survival.

Statistical analysis

All summary statistics (average values, s.d., s.e.m., significant differences between groups) were calculated using Prism (GraphPad Software version 7.05) or Microsoft Excel as appropriate. Statistical significance between groups was determined by unpaired, one-tailed Student's *t*-tests ($P \leq 0.05$ was considered statistically significant). Survival in various groups was compared with Prism using the log-rank (Mantel–Cox) test. SK plots were generated using internally developed software (https://skylineplotter.shinyapps.io/SkyLinePlotter/). Unlike the survival plots generated using Prism, SK plots give dynamic simultaneous presentation of tumor volumes and mouse survival at specific time points.

The ROC analysis was used to measure the predictive power of biomarkers using human PBMC and tumor samples. The ROC curve depicts sensitivities and specificities. The AUC is typically used to measure the predictive power of the biomarker on non-response; it is between 0 and 1. The higher the AUC value, the better the predictive power. If we predicted response and non-response randomly, the AUC would be 0.50. An AUC of 1.0 represents perfect prediction.

Statistical significance between responding and non-responding lesions with regard to the average numbers of PD-$1^{+}$$CD38^{+}$ $CD8^{+}$ T cells in the pre- and posttreatment tumor samples was determined by Student's *t*-test when Gaussian assumption is valid; otherwise, the Wilcoxon rank-sum test was used.

Reporting Summary

Further information on research design is available in the Nature Research Reporting Summary linked to this article.

Data availability

For the clinical data, the cohorts were not collected specifically for this study and are already published. The references describing the participants of the human research and clinical data have been provided in this published article. In vitro, in vivo, flow cytometry and clinical data are included in this published article and its Supplementary Information. All other relevant data are available from the corresponding author upon reasonable request.

Supplementary Material

Refer to Web version on PubMed Central for supplementary material.

Acknowledgements

We acknowledge the Georgia Cancer Center, Augusta University internal support grant to S.N.K. We acknowledge the Lombardi Comprehensive Cancer Center support grant to the Biostatistics and Bioinformatics shared service (P30 CA 051008). We acknowledge the Ludwig Center for Cancer Immunotherapy for financial support for the Immune Monitoring Core Facility at the MSKCC. This research was funded in part through the National Institutes of Health (NIH)/National Cancer Institute (NCI) Cancer Center Support grant no. P30 CA008748, grant no.

NIH/NCI R01 CA056821, the Swim Across America, Ludwig Institute for Cancer Research, Parker Institute for Cancer Immunotherapy and Virginia B. Squiers Foundation to J.W. and T.M. The research related to the human tumor samples was supported by the Cancer Research Institute (N.H.), Adelson Medical Research Foundation (N.H.) and NIH/NCI grant no. R01CA208756 (N.H.). We thank R. Ibrahim, Parker Institute for Cancer Immunotherapy, for reviewing the manuscript.

Competing interests

S.N.K., S.G. and V.V. are inventors on patent application related to work on the methods for detecting and reversing immune therapy resistance and the development of PD-$1^{+}$$CD38^{+}$ $CD8^{+}$ T cells as a predictive and therapeutic biomarker for response/resistance to immune checkpoint blockade therapy. S.N.K. reports an honorarium from Syndax, IO Biotech, BioLine, Northwest Biotherapeutics, Advaxis, EMD Serono, GSK, UbiVac, McKinsey, AstraZeneca and Lycera. S.N.K. reports stocks or ownership interest in Advaxis, GeorgiaImmune, IO Biotech and Northwest Therapeutics. S.N.K. is a consultant for Syndax, IO Biotech, BioLine, Kahr, PDS Biotechnology, AstraZeneca, CytomX, NewLink Genetics, AratingaBio, CanImGuide and Lycera. S.N.K. is a board member for Advaxis. S.N.K. has research contracts with Syndax, IO Biotech, BioLine, AstraZeneca, MedImmune and Lycera. T.M. is a consultant for Leap Therapeutics, Immunos Therapeutics and Pfizer and co-founder of Imvaq Therapeutics. T.M. has equity in Imvaq Therapeutics. T.M. reports grants from Bristol-Myers Squibb, Surface Oncology, Kyn Therapeutics, Infinity Pharmaceuticals, Peregrine Pharmaceuticals, Adaptive Biotechnologies, Leap Therapeutics and Aprea Therapeutics. T.M. is an inventor on patent applications related to work on oncolytic viral therapy, alphavirus-based vaccines, neoantigen modeling, CD40, glucocorticoid-induced TNFR-related protein (GITR), OX40, PD-1 and CTLA-4. J.W. is a consultant for Adaptive Biotechnologies, Advaxis, Amgen, Apricity, Array BioPharma, Ascentage Pharma, Astellas Pharma, Bayer, BeiGene, Bristol-Myers Squibb, Celgene, Chugai Pharmaceutical, Elucida Oncology, Eli Lilly, F Star, Genentech, Imvaq Therapeutics, Janssen, Kleo Pharmaceuticals, Linneaus, MedImmune, Merck, Neon Therapeutics, Ono Pharmaceutical, Polaris Pharma, Polynoma, PsiOxus Therapeutics, PureTech Health, Recepta Biopharma, Sellas Life Sciences, Serametrix, Surface Oncology and Syndax. J.W. reports an honorarium from Esanex and grants/research support from Bristol-Myers Squibb, MedImmune and Genentech. J.W. has equity in Potenza Therapeutics, Tizona Therapeutics, Adaptive Biotechnologies, Elucida Oncology, Imvaq Therapeutics, BeiGene, Trieza Therapeutics, Serametrix and Linneaus. J.W. is an inventor on patent applications related to work on xenogeneic DNA vaccines, alphavirus replicon particles expressing tyrosinase-related protein-2, myeloid-derived suppressor cell assay, Newcastle disease viruses for cancer therapy, genomic signature to identify responders to ipilimumab in melanoma, engineered vaccinia viruses for cancer immunotherapy, anti-CD40 agonist monoclonal antibody fused to monophosphoryl lipid A for cancer therapy, CAR^{+} T cells targeting differentiation antigens as means to treat cancer, anti-PD-1 antibody, anti-CTLA-4 antibodies, anti-GITR antibodies and methods of use thereof. P.W. is a consultant for Leap Therapeutics. G.M.B. reports paid lecturing from Novartis, Takeda Oncology; sponsored research agreements with Takeda Oncology; and consulting with NW Biotherapeutics. R.J.S. reports personal fees from Amgen, Merck, Genentech and Novartis; research grants from Amgen and Merck; and clinical trial support from Merck, Tesaro, Sanofi, Genentech and Novartis during the conduct of the study; and personal fees from Compugen, Replimmune, Array and Syndax outside the submitted work. J.A.W. is an inventor on a US patent application (PCT/US17/53.717) submitted by the University of Texas MD Anderson Cancer Center that covers methods to enhance immune checkpoint blockade responses by modulating the microbiome; reports compensation for speaker's bureau and honoraria from Imedex, Dava Oncology, Omniprex, Illumina, Gilead, PeerView, Physician Education Resource, MedImmune and Bristol-Myers Squibb; serves as a consultant or advisory board member for Roche/Genentech, Novartis, AstraZeneca, GlaxoSmithKline, Bristol-Myers Squibb, Merck, Biothera Pharmaceuticals and Microbiome DX; and receives research support from GlaxoSmithKline, Roche/Genentech, Bristol-Myers Squibb and Novartis. K.T.F. owns equity in Shattuck Labs, Checkmate, X4 Pharmaceuticals; consults for Novartis, Genentech, BMS, Merck, Takeda, Verastem, Checkmate, X4 Pharmaceuticals, Sanofi, Amgen, Incyte, Adaptimmune, Shattuck Labs, Arch Oncology and Apricity; and receives research support from Novartis, Genentech, Sanofi and Amgen. N.H. is a founder and science advisory board member of Neon Therapeutics. All other authors declare no competing interests.

References

1. Kyi C & Postow MA Checkpoint blocking antibodies in cancer immunotherapy. FEBS Lett. 588, 368–376 (2014). [PubMed: 24161671]
2. Topalian SL, Drake CG & Pardoll DM Immune checkpoint blockade: a common denominator approach to cancer therapy. Cancer Cell 27, 450–461 (2015). [PubMed: 25858804]
3. Dong H et al. Tumor-associated B7-H1 promotes T-cell apoptosis: a potential mechanism of immune evasion. Nat. Med 8, 793–800 (2002). [PubMed: 12091876]
4. Iwai Y et al. Involvement of PD-L1 on tumor cells in the escape from host immune system and tumor immunotherapy by PD-L1 blockade. Proc. Natl Acad. Sci. USA 99, 12293–12297 (2002). [PubMed: 12218188]

5. Page DB, Postow MA, Callahan MK, Allison JP & Wolchok JD Immune modulation in cancer with antibodies. Annu. Rev. Med 65, 185–202 (2014). [PubMed: 24188664]
6. Zou W, Wolchok JD & Chen L PD-L1 (B7-H1) and PD-1 pathway blockade for cancer therapy: mechanisms, response biomarkers, and combinations. Sci. Transl. Med 8, 328rv4 (2016).
7. Kleponis J, Skelton R & Zheng L Fueling the engine and releasing the break: combinational therapy of cancer vaccines and immune checkpoint inhibitors. Cancer Biol. Med 12, 201–208 (2015). [PubMed: 26487965]
8. Sharma P, Hu-Lieskovan S, Wargo JA & Ribas A Primary, adaptive, and acquired resistance to cancer immunotherapy. Cell 168, 707–723 (2017). [PubMed: 28187290]
9. Mkrtichyan M et al. Anti-PD-1 antibody significantly increases therapeutic efficacy of Listeria monocytogenes (Lm)-LLO immunotherapy. J. Immunother. Cancer 1, 15 (2013). [PubMed: 24829751]
10. Mkrtichyan M et al. Anti-PD-1 synergizes with cyclophosphamide to induce potent anti-tumor vaccine effects through novel mechanisms. Eur. J. Immunol 41, 2977–2986 (2011). [PubMed: 21710477]
11. Mkrtichyan M et al. B7-DC-Ig enhances vaccine effect by a novel mechanism dependent on PD-1 expression level on T cell subsets. J. Immunol 189, 2338–2347 (2012). [PubMed: 22837483]
12. Karyampudi L et al. Accumulation of memory precursor CD8 T cells in regressing tumors following combination therapy with vaccine and anti-PD-1 antibody. Cancer Res. 74, 2974–2985 (2014). [PubMed: 24728077]
13. Soares KC et al. PD-1/PD-L1 blockade together with vaccine therapy facilitates effector T-cell infiltration into pancreatic tumors. J. Immunother 38, 1–11 (2015). [PubMed: 25415283]
14. Huang AC et al. T-cell invigoration to tumour burden ratio associated with anti-PD-1 response. Nature 545, 60–65 (2017). [PubMed: 28397821]
15. Patsoukis N et al. Immunometabolic regulations mediated by coinhibitory receptors and their impact on T cell immune responses. Front. Immunol 8, 330 (2017). [PubMed: 28443090]
16. Boussiotis VA Molecular and biochemical aspects of the PD-1 checkpoint pathway. N. Engl. J. Med 375, 1767–1778 (2016). [PubMed: 27806234]
17. Zaretsky JM et al. Mutations associated with acquired resistance to PD-1 blockade in melanoma. N. Engl. J. Med 375, 819–829 (2016). [PubMed: 27433843]
18. Philip M et al. Chromatin states define tumour-specific T cell dysfunction and reprogramming. Nature 545, 452–456 (2017). [PubMed: 28514453]
19. Shrimali RK et al. Concurrent PD-1 blockade negates the effects of OX40 agonist antibody in combination immunotherapy through inducing T-cell apoptosis. Cancer Immunol. Res 5, 755–766 (2017). [PubMed: 28848055]
20. Trautmann L et al. Upregulation of PD-1 expression on HIV-specific $CD8^+$ T cells leads to reversible immune dysfunction. Nat. Med 12, 1198–1202 (2006). [PubMed: 16917489]
21. Day CL et al. PD-1 expression on HIV-specific T cells is associated with T-cell exhaustion and disease progression. Nature 443, 350–354 (2006). [PubMed: 16921384]
22. Latchman Y et al. PD-L2 is a second ligand for PD-1 and inhibits T cell activation. Nat. Immunol 2, 261–268 (2001). [PubMed: 11224527]
23. Refaeli Y, Van Parijs L, Alexander SI & Abbas AK Interferon γ is required for activation-induced death of T lymphocytes. J. Exp. Med 196, 999–1005 (2002). [PubMed: 12370261]
24. Lohman BL & Welsh RM Apoptotic regulation of T cells and absence of immune deficiency in virus-infected gamma interferon receptor knockout mice. J. Virol 72, 7815–7821 (1998). [PubMed: 9733817]
25. Overwijk WW et al. gp100/pmel 17 is a murine tumor rejection antigen: induction of “self ”-reactive, tumoricidal T cells using high-affinity, altered peptide ligand. J. Exp. Med 188, 277–286 (1998). [PubMed: 9670040]
26. Chen L & Flies DB Molecular mechanisms of T cell co-stimulation and co-inhibition. Nat. Rev. Immunol 13, 227–242 (2013). [PubMed: 23470321]
27. Rosette C et al. The impact of duration versus extent of TCR occupancy on T cell activation: a revision of the kinetic proofreading model. Immunity 15, 59–70 (2001). [PubMed: 11485738]

28. Vonderheide RH The immune revolution: a case for priming, not checkpoint. Cancer Cell 33, 563–569 (2018). [PubMed: 29634944]
29. Vonderheide RH, Domchek SM & Clark AS Immunotherapy for breast cancer: what are we missing? Clin. Cancer Res 23, 2640–2646 (2017). [PubMed: 28572258]
30. Sade-Feldman M et al. Defining T Cell states associated with response to checkpoint immunotherapy in melanoma. Cell 175, 998–1013 e20 (2018). [PubMed: 30388456]
31. Frey AB & Monu N Signaling defects in anti-tumor T cells. Immunol. Rev 222, 192–205 (2008). [PubMed: 18364003]
32. Rizvi NA et al. Cancer immunology. Mutational landscape determines sensitivity to PD-1 blockade in non-small cell lung cancer. Science 348, 124–128 (2015). [PubMed: 25765070]
33. Eroglu Z et al. High response rate to PD-1 blockade in desmoplastic melanomas. Nature 553, 347–350 (2018). [PubMed: 29320474]
34. Banerjea A, Bustin SA & Dorudi S The immunogenicity of colorectal cancers with high-degree microsatellite instability. World J. Surg. Oncol 3, 26 (2005). [PubMed: 15890075]
35. Vandeven NA & Nghiem P Merkel cell carcinoma: an unusually immunogenic cancer proves ripe for immune therapy. J. Oncol. Pract 12, 649–650 (2016). [PubMed: 27407162]
36. Yokosuka T et al. Programmed cell death 1 forms negative costimulatory microclusters that directly inhibit T cell receptor signaling by recruiting phosphatase SHP2. J. Exp. Med 209, 1201–1217 (2012). [PubMed: 22641383]
37. Acuto O, Di Bartolo V & Michel F Tailoring T-cell receptor signals by proximal negative feedback mechanisms. Nat. Rev. Immunol 8, 699–712 (2008). [PubMed: 18728635]
38. Poltorak M et al. TCR activation kinetics and feedback regulation in primary human T cells. Cell Commun. Signal 11, 4 (2013). [PubMed: 23317458]
39. Pageon SV et al. Functional role of T-cell receptor nanoclusters in signal initiation and antigen discrimination. Proc. Natl Acad. Sci. USA 113, E5454–E5463 (2016). [PubMed: 27573839]
40. Lee J, Ahn E, Kissick HT & Ahmed R Reinvigorating exhausted T Cells by blockade of the PD-1 pathway. For. Immunopathol. Dis. Therap 6, 7–17 (2015).
41. Schietinger A et al. Tumor-specific T cell dysfunction is a dynamic antigen-driven differentiation program initiated early during tumorigenesis. Immunity 45, 389–401 (2016). [PubMed: 27521269]
42. Chatterjee S et al. CD38-NAD^+ axis regulates immunotherapeutic anti-tumor T cell response. Cell Metab. 27, 85–100.e8 (2018). [PubMed: 29129787]
43. Mason EF & Rathmell JC Cell metabolism: an essential link between cell growth and apoptosis. Biochim. Biophys. Acta 1813, 645–654 (2011). [PubMed: 20816705]
44. Thommen DS et al. A transcriptionally and functionally distinct $PD\text{-}1^+$ $CD8^+$ T cell pool with predictive potential in non-small-cell lung cancer treated with PD-1 blockade. Nat. Med 24, 994–1004 (2018). [PubMed: 29892065]
45. Blackburn SD, Shin H, Freeman GJ & Wherry EJ Selective expansion of a subset of exhausted CD8 T cells by αPD-L1 blockade. Proc. Natl Acad. Sci. USA 105, 15016–15021 (2008). [PubMed: 18809920]
46. Patel SP & Kurzrock R PD-L1 expression as a predictive biomarker in cancer immunotherapy. Mol. Cancer Ther 14, 847–856 (2015). [PubMed: 25695955]
47. Li Y et al. Prognostic impact of programed cell death-1 (PD-1) and PD-ligand 1 (PD-L1) expression in cancer cells and tumor infiltrating lymphocytes in colorectal cancer. Mol. Cancer 15, 55 (2016). [PubMed: 27552968]
48. Sabatier R et al. Prognostic and predictive value of PDL1 expression in breast cancer. Oncotarget 6, 5449–5464 (2015). [PubMed: 25669979]
49. Jiang P et al. Signatures of T cell dysfunction and exclusion predict cancer immunotherapy response. Nat. Med 24, 1550–1558 (2018). [PubMed: 30127393]
50. Buchwald ZS et al. Radiation, immune checkpoint blockade and the abscopal effect: a critical review on timing, dose and fractionation. Front. Oncol 8, 612 (2018). [PubMed: 30619752]
51. Eisenhauer EA et al. New response evaluation criteria in solid tumours: revised RECIST guideline (version 1.1). Eur. J. Cancer 45, 228–247 (2009). [PubMed: 19097774]

52. Villani AC Single-cell RNA-seq reveals new types of human blood dendritic cells, monocytes, and progenitors. Science 356, eaah4573 (2017). [PubMed: 28428369]

53. Ji Y et al. Identification of the genomic insertion site of Pmel-1 TCR α and β transgenes by next-generation sequencing. PLoS ONE 9, e96650 (2014). [PubMed: 24827921]

54. Lin KY et al. Treatment of established tumors with a novel vaccine that enhances major histocompatibility class II presentation of tumor antigen. Cancer Res. 56, 21–26 (1996). [PubMed: 8548765]

55. Abu Eid R et al. Akt1 and −2 inhibition diminishes terminal differentiation and enhances central memory CD8+ T-cell proliferation and survival. Oncoimmunology 4, e1005448 (2015). [PubMed: 26155399]

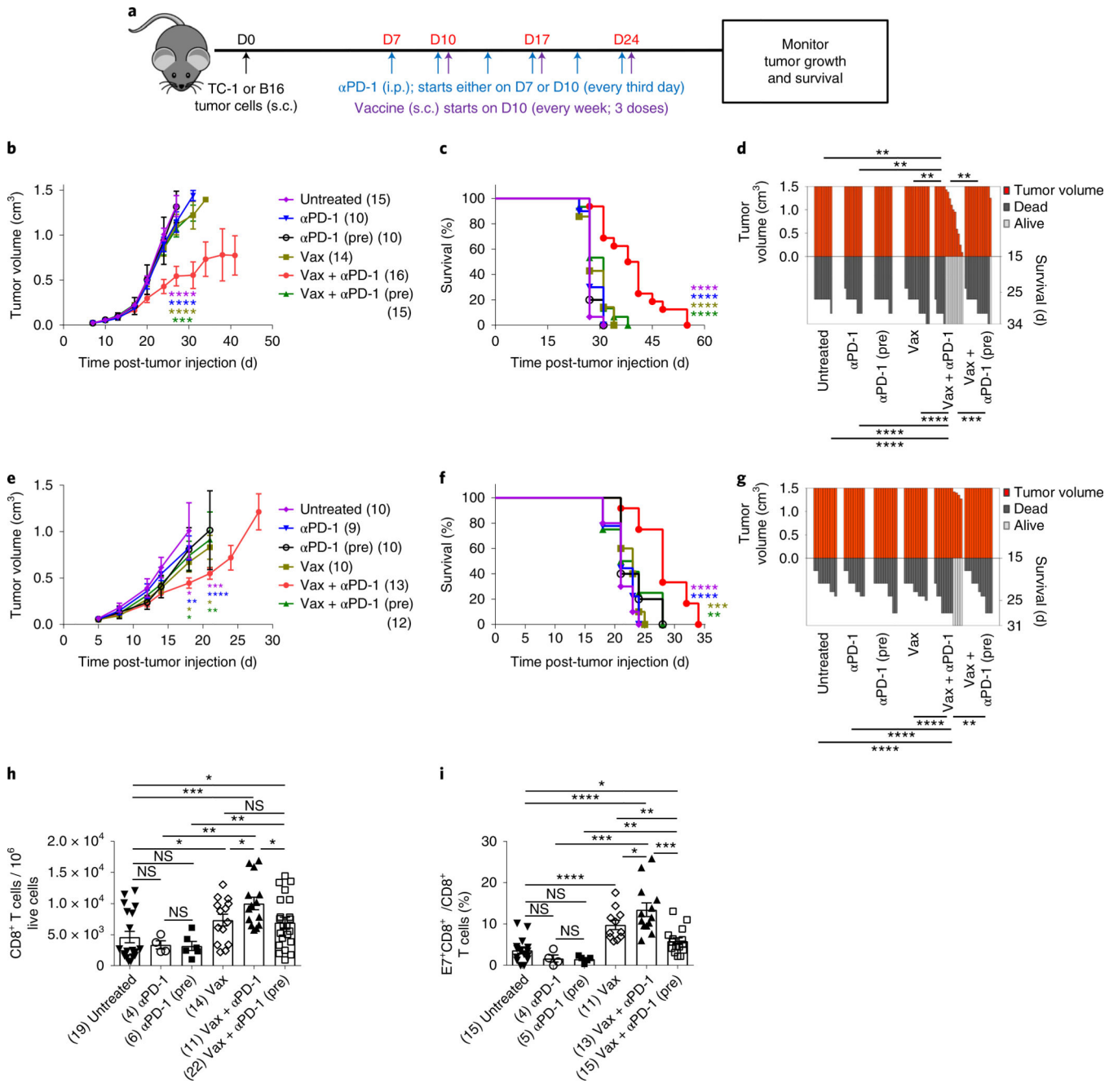

Fig. 1 |. Anti-PD-1 before antigenic stimulation abrogates the antitumor effects of Vax + αPD-1.

a, Schedule of mouse treatments. **b**–**g**, Tumor growth profiles (**b**,**e**), mouse survival (**c**,**f**) and SK plots (**d**,**g**) after various treatments in TC-1 (**b**–**d**) and B16 (**e**–**g**) tumor models. Tumor growth and survival data are the average of two independent experiments with the indicated numbers of mice per group. The error bars indicate the s.e.m. For tumor growth, statistical analysis was performed by unpaired, one-tailed Student's *t*-test, with the asterisks colored to indicate the comparison: purple, comparison to untreated; blue, comparison to anti-PD-1; brown, comparison to Vax; green, comparison to Vax + anti-PD-1 (pre). Individual P values (for the same order of comparisons) are as follows: ***$P = 0.001$, ****$P \leq 0.0001$ (**b**). **P

= 0.0078, $**P = 0.0078$, $**P = 0.0022$ and $**P = 0.0016$ (day (D) 34) (**d**). $*P = 0.0244$, $**P = 0.0037$, $*P = 0.0313$ and $*P = 0.0451$ (day 18); $***P = 0.0001$, $****P \leq 0.0001$, $*P = 0.0262$ and $**P = 0.0086$ (day 21) (**e**). Survival in various groups was compared using log-rank (Mantel–Cox) tests. Individual *P* values (for the same order of comparisons except where indicated) are as follows: $****P \leq 0.0001$ (all comparisons) (**c**); $****P \leq 0.0001$, $****P \leq 0.0001$, $****P \leq 0.0001$, $***P = 0.0003$ (day 34) (**d**); $****P \leq 0.0001$, $****P \leq 0.0001$, $***P = 0.0002$, $**P = 0.0027$ (**f**); $****P \leq 0.0001$, $****P \leq 0.0001$, $***P = 0.0002$, $**P = 0.0027$ (day 31) (**g**). **h**,**i**, Profiles of total $CD8^+$ (**h**) and antigen-specific $CD8^+$ T cells (**i**) in the TME of TC-1-bearing mice after various treatments, 3 d after the second vaccination (D20). Flow cytometry data are the average from two independent experiments. Each dot corresponds to one mouse with the indicated number of mice per group given in parentheses. The error bars indicate the s.e.m. Statistical analysis was performed by unpaired, one-tailed Student's t-test. Individual *P* values are as follows: $*P = 0.0255$ (left), $*P = 0.0322$ (middle), $*P = 0.0146$ (right), $*P = 0.0365$ (upper), $**P = 0.0018$ (lower), $**P = 0.01$ (upper), $***P = 0.0002$ (**h**). $*P = 0.0059$ (lower), $*P = 0.0273$ (upper), $**P = 0.0035$ (lower), $**P = 0.0039$ (upper), $***P = 0.0008$ (left), $***P = 0.0001$ (right), $****P \leq 0.0001$ (**i**). NS, not significant; $*P \leq 0.05$; $**P \leq 0.01$; $***P \leq 0.001$; $****P \leq 0.0001$.

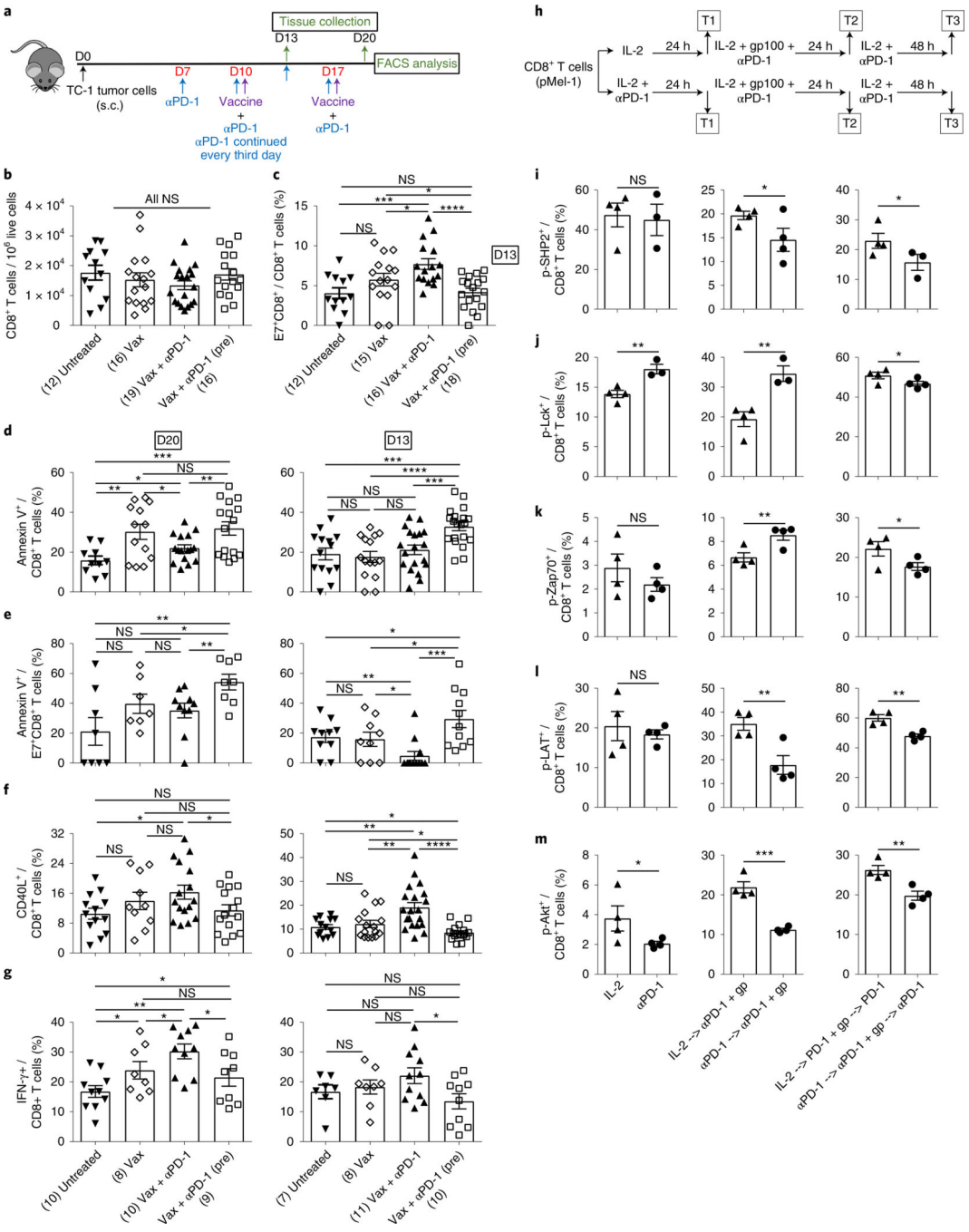

Fig. 2 |. Prior PD-1 blockade abrogates vaccine-induced tumor-specific immune responses early during the course of treatment.

a, Schedule of mouse treatments. Tumor tissues were collected 3 d after priming (day 13) or 3 d after boosting (day 20). **b**,**c**, Numbers of total (**b**) and antigen-specific $CD8^+$ T (**c**) cells at day 13. **d**,**e**, Frequencies of annexin V^+ total (**d**) and antigen-specific $CD8^+$ T (**e**) cells in the TME at days 20 and 13, as shown. **f**,**g**, Frequencies of $CD40L^+$ (**f**) and IFN-γ^+ (**g**) $CD8^+$ T cells in the TME at days 20 and 13 as shown. Flow cytometry data are the average from two independent experiments. Each dot corresponds to one mouse with the indicated number

of mice per group given in parentheses. The error bars indicate the s.e.m. For statistical comparison, an unpaired, one-tailed Student's *t*-test was used. NS (**b**); **P* = 0.0344 (lower), **P* = 0.0448 (upper), ****P* = 0.0005, *****P* ≤ 0.0001 (**c**); **P* = 0.0229 (lower), **P* = 0.0179 (upper), ***P* = 0.0033 (left), ***P* = 0.0068 (right), ****P* = 0.001 (left panel); ****P* = 0.0004 (lower), ****P* = 0.0002 (upper), *****P* ≤ 0.0001 (right panel) (**d**); **P* = 0.0498, ***P* = 0.009 (lower), ***P* = 0.0038 (upper) (left panel); **P* = 0.0254 (lower), **P* = 0.0479 (middle), **P* = 0.0496 (top), ***P* = 0.0067, ****P* = 0.0004 (right panel) (**e**); **P* = 0.0138 (left), **P* = 0.0274 (right) (left panel); **P* = 0.0187 (lower), **P* = 0.0339 (upper), ***P* = 0.0063 (lower), ***P* = 0.002 (upper), *****P* ≤ 0.0001 (right panel) (**f**); **P* = 0.0264 (left), **P* = 0.05 (middle), **P* = 0.0177(right), **P* = 0.05 (top), ****P* = 0.0002 (left panel); **P* = 0.015 (right panel) (**g**). **h**, Experimental outline for Pmel-1 $CD8^+$ T cell treatment. T1, T2 and T3 refer to various time points during the course of treatment when samples were picked for analysis. **i**–**m**. Flow cytometry analysis of phosphorylated $SHP2^+$ (**i**), Lck^+ (**j**), $Zap70^+$ (**k**), LAT^+ (**l**) and Akt^+ (**m**) $CD8^+$ T cells at three time points. Data are representative of two independent experiments with at least 3–4 technical replicates per group. The error bars indicate the s.e.m. For comparisons, an unpaired, one-tailed Student's *t*-test was used. T1: NS; T2: **P* = 0.0466; T3: **P* = 0.05 (**i**); T1: ***P* = 0.0042; T2: ***P* = 0.0043; T3: **P* = 0.0457 (**j**); T1: NS; T2: ***P* = 0.0086; T3: **P* = 0.0363 (**k**); T1: NS; T2: ***P* = 0.0054; T3: ***P* = 0.0017 (**l**); T1: **P* = 0.048; T2: ****P* = 0.0002; T3: ***P* = 0.0034 (**m**). **P* ≤ 0.05; ***P* ≤ 0.01; ****P* ≤ 0.001; *****P* ≤ 0.0001.

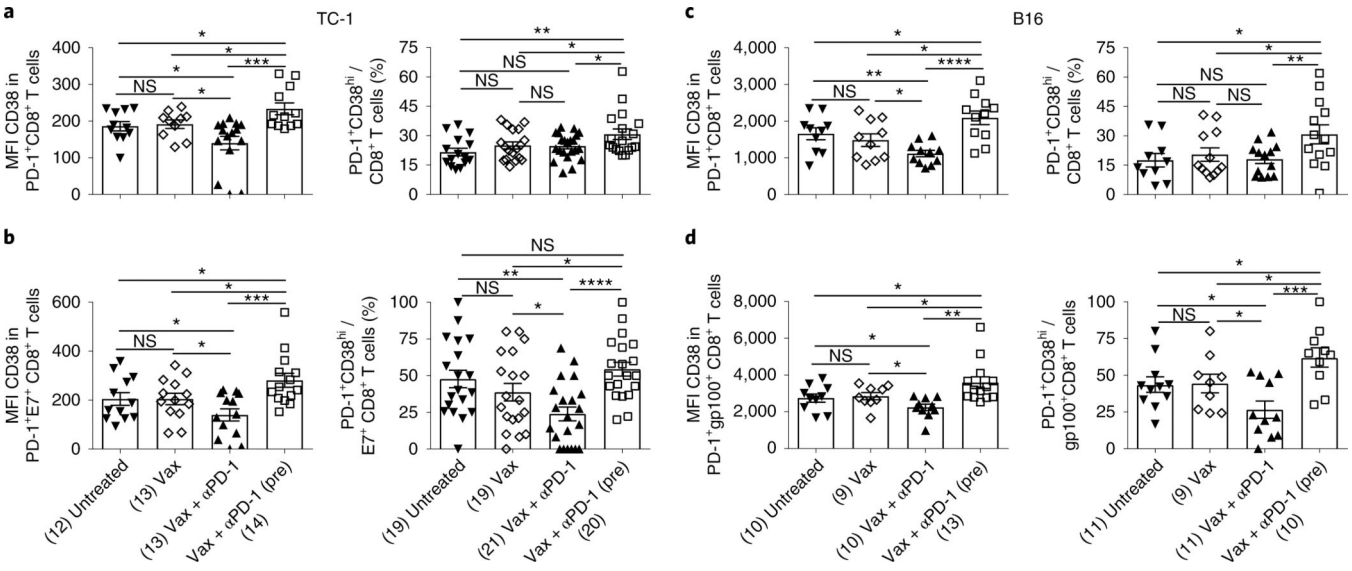

Fig. 3 |. PD-1 blockade before antigenic stimulation induces PD-1^{+}CD38^{hi} CD8^{+} T cells.

a–**d**, MFI and frequency of PD-1^{+}CD38^{hi} T cells in total (**a**,**c**) and antigen-specific (**b**,**d**) CD8^{+} T cells in TC-1 (**a**,**b**) and B16 (**c**,**d**) tumor-bearing mice at day 13 post-tumor implantation. Data are the average of two independent experiments. Each dot corresponds to one mouse with the indicated number of mice per group given in parentheses. The error bars indicate the s.e.m. For statistical comparison, an unpaired, one-tailed Student's *t*-test was used. NS; versus untreated: **P* = 0.0339 (lower) and **P* = 0.0164 (upper); versus Vax: **P* = 0.0233 (lower) and **P* = 0.0269 (upper), ****P* = 0.0005 (left panel); **P* = 0.0201 (lower), **P* = 0.0416 (upper), ***P* = 0.006 (right panel) (**a**); versus untreated: **P* = 0.0416 (lower) and **P* = 0.0316 (upper); versus Vax: **P* = 0.0342 (lower) and **P* = 0.0261 (upper), ****P* = 0.0005 (left panel); **P* = 0.028 (lower), **P* = 0.0221 (upper), ***P* = 0.0015, *****P* ≤ 0.0001 (right panel) (**b**); **P* = 0.032 (lower), **P* = 0.0137 (middle), **P* = 0.0482 (upper), ***P* = 0.0037, *****P* ≤ 0.0001 (left panel); **P* = 0.0498 (lower), **P* = 0.0241 (upper), ***P* = 0.01 (right panel) (**c**); versus untreated: **P* = 0.0478 (lower) and **P* = 0.0273 (upper); versus Vax: **P* = 0.0168 (lower) and **P* = 0.0464 (upper), ***P* = 0.0014 (left panel); versus untreated: **P* = 0.0213 (lower) and **P* = 0.0202 (upper); versus Vax: **P* = 0.0272 (lower) and * *P* = 0.035 (upper), ****P* = 0.0003 (right panel) (**d**). **P* ≤ 0.05; ***P* ≤ 0.01; ****P* ≤ 0.001; *****P* ≤ 0.0001.

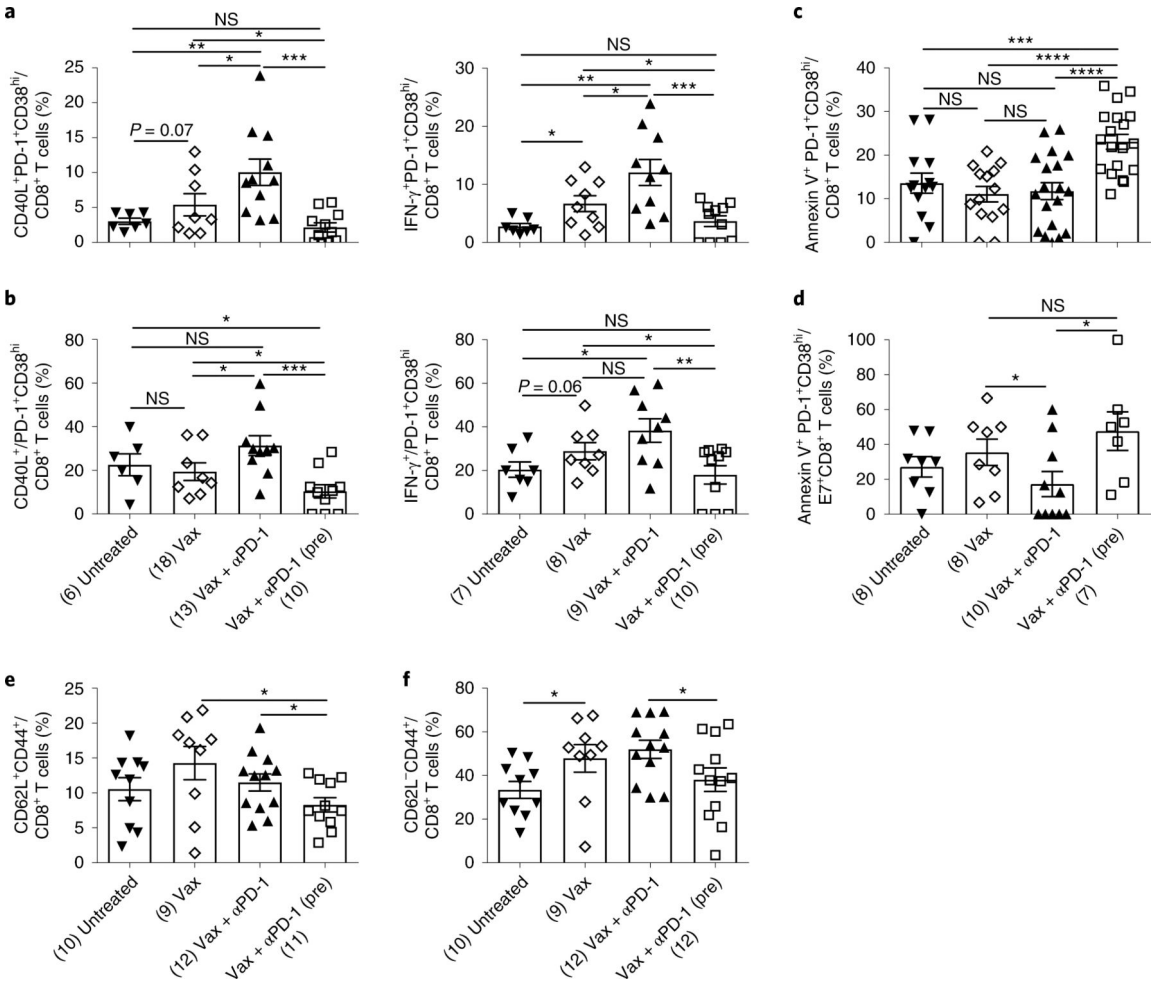

Fig. 4 |. PD-1^{+}CD38^{hi} CD8^{+} T cells induced as a result of anti-PD-1 pretreatment are dysfunctional.

a,**b**, Frequency of CD40L^{+} or IFN-γ^{+} PD-1^{+}CD38^{hi} cells in total CD8^{+} T cells (**a**) and in the PD-1^{+}CD38^{hi} CD8^{+} T cell population (**b**). **c**,**d**, Frequencies of annexin V^{+} PD-1^{+}CD38^{hi} cells in total (**c**) and antigen-specific (**d**) CD8^{+} T cells. **e**,**f**, Frequencies of CD62L^{+}CD44^{+} (**e**) and CD62L^{-}CD44^{+} (**f**) CD8^{+} T cells after various treatments as shown. Data at day 13 (**a**–**d**) and day 20 (**e**,**f**) post-TC-1 tumor implantation. Data are representative of two independent experiments. Each dot corresponds to one mouse with the indicated number of mice per group given in parentheses. The error bars indicate the s.e.m. For comparison purposes, an unpaired, one-tailed Student's *t*-test was used. *P = 0.0462 (lower), *P = 0.0258 (upper), **P = 0.0052, ***P = 0.0004 (left panel); *P = 0.0148 (lower), *P = 0.0309 (middle), *P = 0.0382 (upper), **P = 0.002, ***P = 0.001 (right panel) (**a**); *P = 0.0372 (lower), *P = 0.0449 (middle), *P = 0.0225 (upper), ***P = 0.0006 (left panel); *P = 0.0104 (lower), *P = 0.0421 (upper), **P = 0.004 (right panel) (**b**); ***P = 0.001, ****$P \leq$ 0.0001 (**c**); *P = 0.05 (lower), *P = 0.0146 (upper) (**d**); *P = 0.0299 (lower), *P = 0.012 (upper) (**e**); *P = 0.0318 (left), *P = 0.0271 (**f**) (right). *$P \leq$ 0.05; **$P \leq$ 0.01; ***$P \leq$ 0.001; ****$P \leq$ 0.0001.

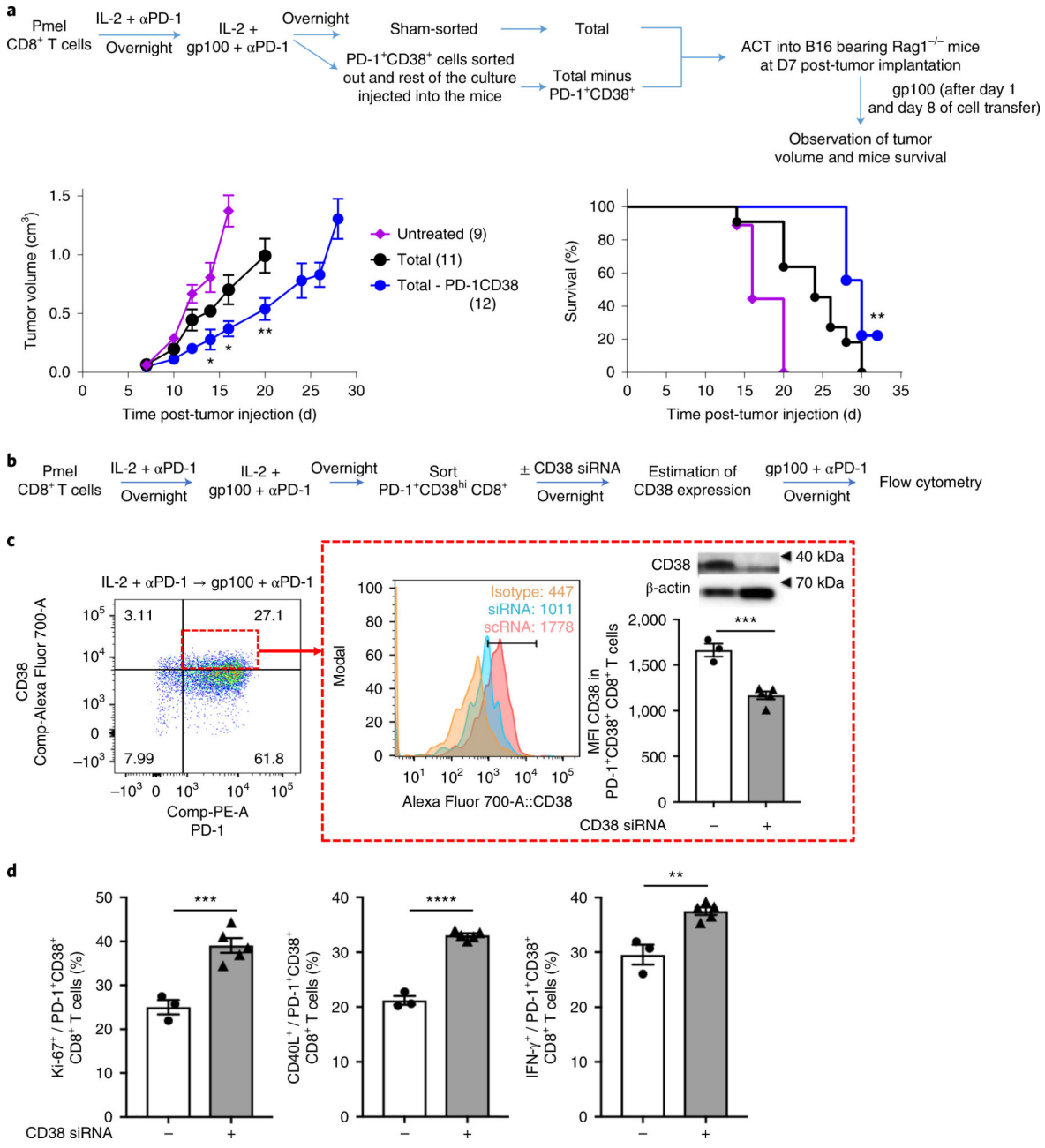

Fig. 5 |. Depletion of PD-1^{+}CD38^{hi} CD8^{+} T cells results in a strong antitumor response.

a, Tumor growth and survival of variously treated B16-bearing *Rag1*$^{-/-}$ mice following transfer of either total or PD-1^{+}CD38^{+}-depleted, in vitro-activated CD8^{+} T cells (with the indicated number of mice per group given in parentheses); data are the average of two independent experiments. The error bars indicate the s.e.m. Left panel: for comparison purposes, an unpaired, one-tailed Student's *t*-test was used; **P* = 0.017 (day 14), **P* = 0.0127 (day 16), ***P* = 0.0074 (day 20). Right panel: survival in various groups was compared using the log-rank (Mantel–Cox) test; ***P* = 0.0054. **b**, Experimental outline for Pmel-1 CD8^{+} T cell treatment. **c**, MFI and protein expression of CD38 in PD-1^{+}CD8^{+} T cells (shown in the small red box on the left). The protein expression of CD38 in flow-sorted

PD-1^{+}CD38^{+} T cells transfected with CD38 siRNA or scrambled RNA (scRNA) was determined by immunoblot. The expression of β-actin was used as a loading control (the uncropped full scan of the blot is shown in Supplementary Fig. 5b). **d**, Frequency of Ki-67^{+}, CD40L^{+} and IFN-γ^{+} in the PD-1^{+}CD38^{+} CD8^{+} T cell population. Data are representative of two independent experiments with at least 3–5 technical replicates per group. The error bars indicate the s.e.m. For comparison purposes, an unpaired, one-tailed Student's *t*-test was used. ***$P = 0.0003$ (**c**); ***$P = 0.0007$ (left panel); ****$P \leq 0.0001$ (middle panel); **$P = 0.0012$ (right panel) (**d**). *$P \leq 0.05$; **$P \leq 0.01$; ***$P \leq 0.001$; ****$P \leq 0.0001$.

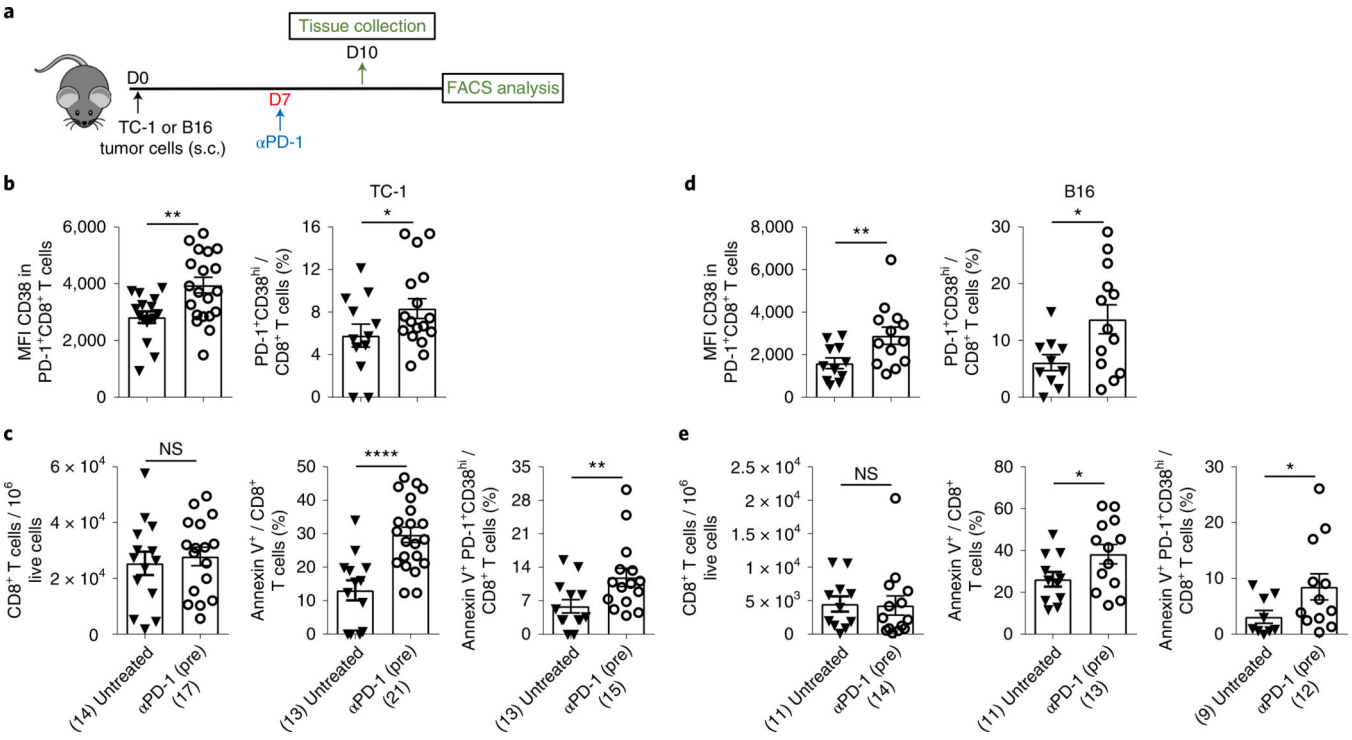

Fig. 6 |. PD-1 blockade without proper priming predisposes CD8$^+$ T cells toward dysfunction and apoptosis-mediated cell death.

a, Schedule of mouse treatment. **b**–**e**, Estimation of CD38 MFI and frequency of PD-1$^+$CD38^{hi} CD8$^+$ T cells (**b**,**d**) and frequency of total CD8$^+$, Annexin V$^+$ CD8$^+$ and Annexin V$^+$ PD-1$^+$CD38^{hi} CD8$^+$ T cells (**c**,**e**) in variously treated TC-1 (**b**,**c**) and B16 (**d**,**e**) tumor-bearing mice. Day 10 data after tumor implantation; data are the average of two independent experiments. Each dot corresponds to one mouse with the indicated number of mice per group given in parentheses. The error bars indicate the s.e.m. For comparison purposes, an unpaired, one-tailed Student's *t*-test was used. *P = 0.0201 (left panel), *P = 0.0435 (right panel) (**b**); NS (left panel); ****$P \leq 0.0001$ (middle panel); **P = 0.0096 (right panel) (**c**); **P = 0.0083 (left panel), *P = 0.0129 (right panel) (**d**); NS (left panel), *P = 0.0291 (middle panel), *P = 0.0392 (right panel) (**e**). *$P \leq 0.05$; **$P \leq 0.01$; ***$P \leq 0.001$; ****$P \leq 0.0001$.

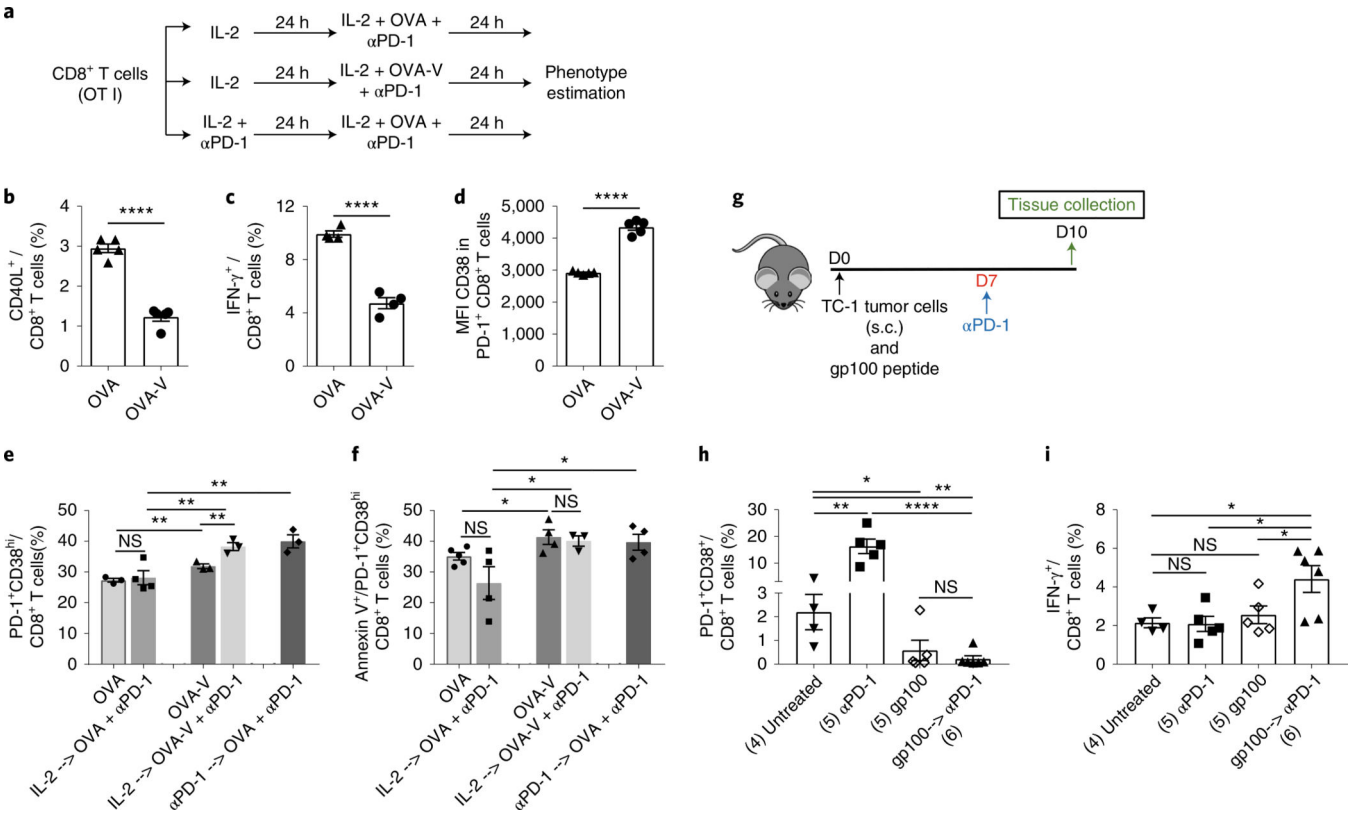

Fig. 7 |. PD-1 blockade in suboptimally primed CD8$^+$ T cells induces dysfunctional PD-1$^+$CD38^{hi} CD8$^+$ T cells.

a, Treatment schedule for in vitro activation of OT I CD8$^+$ T cells with OVA or OVA-V as indicated. **b,c**, Frequency of CD40L$^+$ (**b**) and IFN-γ^+ (**c**) CD8$^+$ T cells after various treatments. **d**, MFI of CD38 in PD-1$^+$ CD8$^+$ T cells. **e**, Frequency of PD-1$^+$CD38^{hi} cells in CD8$^+$ T cells after various treatments. **f**, Frequency of annexin V$^+$ cells in PD-1$^+$CD38^{hi} CD8$^+$ T cells after various treatments. In vitro data are representative of two independent experiments with at least four technical replicates. **g**, Schedule of mouse treatment. **h**,**i**, Frequency of PD-1$^+$CD38^{hi} (**h**) and IFN-γ^+ (**i**) CD8$^+$ T cells after various treatments in TC-1 tumor-bearing mice. Day 10 data after tumor implantation; data are representative of one of two independent experiments. Each dot corresponds to one mouse with the indicated number of mice per group given in parentheses. The error bars indicate the s.e.m. For comparison purposes, an unpaired, one-tailed Student's *t*-test was used. ****$P \leq 0.0001$ (**b**); ****$P \leq 0.0001$ (**c**); ****$P \leq 0.0001$ (**d**); NS, OVA versus OVA-V: **$P = 0.0047$, **$P = 0.0067$ (lower), **$P = 0.009$ (middle), **$P = 0.0073$ (upper) (**e**); *$P = 0.0211$ (lower), *$P = 0.0436$ (middle), *$P = 0.0328$ (upper) (**f**); *$P = 0.044$, **$P = 0.0015$ (left), **$P = 0.0061$ (right), ****$P \leq 0.0001$ (**h**); *$P = 0.0312$ (lower), *$P = 0.0112$ (middle), *$P = 0.0172$ (upper) (**i**). *$P \leq 0.05$; **$P \leq 0.01$; ***$P \leq 0.001$; ****$P \leq 0.0001$.

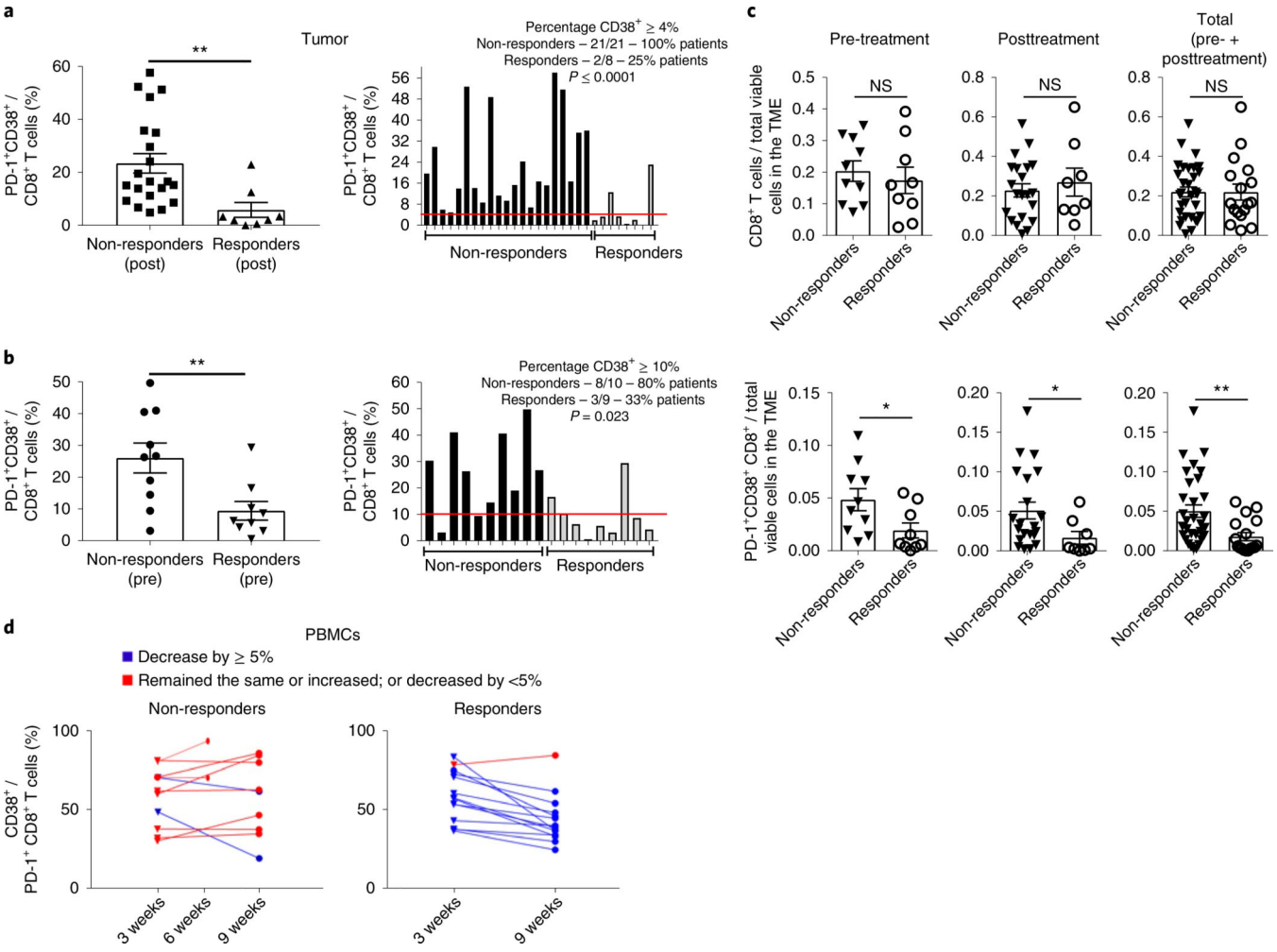

Fig. 8 |. The frequency of PD-1$^+$CD38$^+$ CD8$^+$ T cells is a pharmacodynamic and predictive biomarker of anti-PD-1 therapy.

a, The posttreatment average frequency of PD-1$^+$CD38$^+$ CD8$^+$ T cells in 21 non-responding and 8 responding tumor lesions, as determined by single-cell RNA sequencing analysis, is shown on the left and the individual frequencies are shown on the right. The red line depicts the cutoff limit where at least 4% or more CD8$^+$ T cells were PD-1$^+$CD38$^+$ in the tumors. **b**, The pretreatment average frequency of PD-1$^+$CD38$^+$ CD8$^+$ T cells in 10 non-responding and 9 responding tumors lesions is shown on left and the individual frequencies are shown on the right. The red line depicts the cutoff limit where at least 10% or more CD8$^+$ T cells were PD-1$^+$CD38$^+$ in the tumors. The error bars indicate the s.e.m. Left panels: an unpaired, one-tailed Student's *t*-test was used. $^{**}P = 0.0045$ (**a**); $^{**}P = 0.0048$ (**b**). The post- and pretreatment cutoffs that best predicted responders from non-responders were determined a priori and were further confirmed using ROC analysis (right panels). **c**, Absolute numbers of CD8$^+$ (top) and PD-1$^+$CD38$^+$ CD8$^+$ (bottom) T cells in total viable cells in the TME in the pretreatment (non-responders: $n = 10$; responders: $n = 9$), posttreatment (non-responders: $n = 21$; responders: $n = 8$) or total (non-responders: $n = 31$; responders: $n = 17$) number of responding and non-responding tumor lesions. Each dot corresponds to one tumor lesion. The error bars indicate the s.e.m. For comparison purposes, a one-tailed Student's *t*-test was

used. Top panels: NS; bottom panels: $*P = 0.019$ (pretreatment); $*P = 0.034$ (posttreatment); $**P = 0.0034$ (total). **d**, Flow cytometry measurements of $CD38^+$ cells in $PD\text{-}1^+CD8^+$ T cells in PBMCs from advanced melanoma patients at 3 and 9 weeks after anti-PD-1 treatment. For two non-responding patients, data are shown at 6 weeks since samples were not available at week 9.